EVOLUTION IN H_2O CONTENTS DURING DEFORMATION OF POLYCRYSTALLINE QUARTZ: AN EXPERIMENTAL STUDY

ABSTRACT

Shear experiments were performed in a Griggs-type apparatus at 800°C and 1.5GPa, at a strain rate of 2.1 x $10^{-5}s^{-1}$ using different starting materials: (i) Powder (grain size 6-10μm) of dry Brazil quartz with 0.15wt% added H_2O, (ii) "dry" Brazil quartz porphyroclasts (grain size ~100-200μm), devoid of fluid inclusions embedded in the same fine grained powder, and (iii) "wet" porphyroclasts (grain size ~100-200μm), containing initially a high density of μm-scale fluid inclusions embedded in the same powder. After hot pressing, samples were deformed to large shear strains (γ~3 to 4.5), in order for the microstructures and H_2O distribution to approach some state of "equilibrium". The H_2O content and speciation in quartz were analyzed by Fourier Transform Infra-Red (FTIR) spectroscopy before and after the experiments. Mechanical peak strength is generally lower in experiments with 100% hydrated matrix, intermediate in experiments incorporating wet porphyroclasts (with a proportion of 30 or 70%) and highest in those with dry porphyroclasts. All experiments with porphyroclasts show pronounced strain weakening, and the strengths of most samples converge to similar values at large strain. Wet porphyroclasts are pervasively recrystallized during deformation, while dry porphyroclasts recrystallize only at their rims and remain weakly deformed. Recrystallization of the initially fluid-inclusion-rich porphyroclasts results in a decrease in inclusion abundance and total H_2O content, while H_2O content of initially dry clasts increases during deformation. H_2O contents of all high strain samples converge to similar values for matrix and recrystallized grains. In samples with wet porphyroclasts, shear bands with high porosity and fluid contents develop and they host the precipitation of euhedral quartz crystals surrounded by a free-fluid phase. These high porosity sites are sinks for collecting H_2O in excess of the storage capacity of the grain boundary network of the recrystallized aggregate. The H_2O storage capacity of the grain boundary network is determined as a H_2O-boundary-film of ~0.7 nm thickness.

1. INTRODUCTION

Quartz weakening by H_2O is well known since the seminal papers by Griggs and Blacic (1965) and Griggs (1967). In natural rocks, it is tacitly assumed that quartz is sufficiently "wet", because quartz usually is one of the weakest components in plastically deformed rocks. However, some recent observations have described potentially drier natural rocks, which are deformed (Fitzgerald et al., 2006, Menegon et al., 2011, Kilian et al., 2016). On the other hand, there is clear evidence for shear zones involving material initially rich in H_2O (principally in the form of fluid inclusions), such as metasediments along the subduction plate interface (Palazzin et al., 2016; Raimbourg et al., 2018; Raimbourg et al., 2015, Saffer and Tobin, 2011), and the final deformed rocks do not necessarily indicate high H_2O contents. Thus, the introduction or reduction of H_2O in quartz in natural rock deformation remains one of the great unknown parameters.

As pointed out by Griggs (1967), the H_2O weakening effect in quartz may combine different elementary processes, which all contribute to enhance plastic deformation. One process is related to the enhanced intra-crystalline plasticity of quartz. It has been extensively studied in single crystals, most of them synthetic (Griggs, 1967, 1974; Griggs and Blacic, 1965; Kekulawala et al., 1978, 1981; McLaren et al., 1983; McLaren et al., 1989). The microscopic weakening phenomenon may eventually depend on the hydrolysis of Si-O bonds in the cores of dislocations (Griggs, 1974), on enhanced climb of dislocations (Cordier and Doukhan, 1989; Mainprice and Jaoul, 2009; Tullis and Yund, 1989), or involve the increased dislocation nucleation at nano-scale H_2O clusters acting as dislocation sources (Fitz Gerald et al., 1991; McLaren et al., 1989). H_2O, in the form of molecular H_2O is most efficient to weaken quartz single crystals (e.g., Paterson, 1989, Kekulawala et al., 1978, 1981). However, the growth of nano-scale clusters of H_2O to form larger fluid inclusions, resulting from heat treatment, increases quartz strength (Kekulawala et al., 1978): milky quartz containing a large concentration of H_2O confined in µm-scale fluid inclusions is stronger than synthetic crystal with a much lower H_2O concentration. The effect of OH structural defects on deformation is unclear but appears limited (Doukhan and Trépied, 1985; Paterson, 1989; Kronenberg, 1994; Cordier et al., 1994). However, in a given quartz material, the weakening effect increases with the H_2O content (Griggs, 1967, Blacic and Christie, 1984, Kronenberg and Tullis, 1984, Cordier and Doukhan 1989, Hirth and Tullis 1992, Den Brok et al.,1994, Stunitz et al., 2017).

Another elementary process, proposed by Griggs (1967) as a cause of quartz hydrolytic weakening, is recrystallization, which operates in polycrystals (Jaoul et al., 1984; Tullis and Yund, 1989; Hirth and Tullis, 1992). Similar to single crystals, in quartz aggregates, there is an inverse correlation between the amount of added H_2O and the assemblage strength (Jaoul et al., 1984; Kronenberg and Tullis, 1984). In particular, in H_2O-rich experiments, the small grain sizes decrease strength, suggesting some contribution of grain-boundary mediated process to weakening (Kronenberg and Tullis, 1984).

The case of deformation of polycrystalline material is of prime interest to nature, as it directly applies to the strength of mylonites and ultramylonites. It involves the combination of intracrystalline and grain boundary processes, so that identifying the H_2O-weakening effect is difficult. In addition, natural material may contain H_2O concentrations varying over several orders of magnitude (Ito and Nakashima, 2002): microcrystalline cherts, non-metamorphic or of diagenetic grade, contain up to ~40,000 H/10^6Si. In contrast, the threshold for the onset of weakening, in other words the boundary between wet and dry quartz in experiments on synthetic quartz, is ~100 H/10^6 Si (Griggs and Blacic, 1965; Cordier and Doukhan, 1991, Den Brock, 1994; Christie et al., 1964, Kilian et al., 2016). Not all of the H_2O content of natural quartz (primarily in µm-scale fluid inclusions) has a weakening effect (Kekulawala et al., 1978), but the mechanical role of large H_2O concentrations is still to be determined.

In particular, considering natural quartz as a two-phase-system of crystal and fluid inclusions, the transfer of H_2O from the inclusions into the crystal (and the associated weakening) is difficult because of the very low solubility and diffusive flux of H_2O in quartz (Kronenberg et al., 1986, Paterson 1986, Gerretsen et al., 1989). As a consequence, micro-fracturing (Kronenberg et al., 1986, 1990, Gerretsen et al., 1989, FitzGerald et al., 1991, Stunitz et al., 2017) and diffusion (along subgrain boundaries or dislocation cores; Post and Tullis, 1998)), as well as grain boundary migration (Gleason and DeSisto, 2008), have been proposed as mechanisms responsible for H_2O uptake, because oxygen diffusion may be increased along dislocations or grain boundaries.

Finally, H_2O concentration is not a fixed quantity and depends itself on deformation, as recrystallization redistributes H_2O within the material. For example, in rock of low metamorphic grade from Japanese accretionary complexes, the H_2O concentration decreases with increasing grade, reflecting the progress of recrystallization (Ito and Nakashima, 2002). In grains with a large initial H_2O content stored in fluid inclusions, the migration of grain boundaries that accompanies recrystallization leads to the loss of most fluid inclusions and the decrease H_2O concentration (Bakker and Jansen, 1994; Kilian et al., 2016; Palazzin et al., 2016). Therefore, the "steady-state" H_2O concentration (and the associated strength) in a deforming and recrystallizing aggregate is poorly known. FTIR measurements in natural mylonites formed at mid-greenschist and amphibolite facies conditions show low H_2O contents, <100 to ~320 H/10^6 Si at grain boundary regions (Gleason and DeSisto, 2008) and in individual single grains (Kilian et al., 2016).

Given the wealth of existing experimental and natural studies on H_2O weakening of quartz, this study specifically focuses on the strength of quartz as a function of H_2O-content. Another aspect of this study is the evolution of H_2O-content (i.e. increasing and decreasing H_2O contents in deforming polycrystals). "Wet" initial conditions (e.g., applicable to examples to sediments in subduction settings) and dry initial crystals are compared and their H_2O-evolution studied. We have carried out high strain experiments in order to simulate natural shear zones but also to be as close as possible to steady-state conditions, both in terms of microstructures and H_2O distribution. We focused on the role of H_2O on recrystallization and the effect of H_2O content and speciation.

2. METHODS

2.1 Experimental procedure

All experiments were performed in a Griggs-apparatus at 800°C, ~1500 MPa and a constant strain rate of ~2 $x10^{-5}$ s^{-1}. These conditions were chosen in order to activate dislocation creep in the samples (cf. Hirth and Tullis, 1992). Pre-cut (at 45°) Al_2O_3 pistons were inserted into a pre-annealed platinum jacket. A ~1mm thick layer of fine quartz matrix powder was placed between pistons, which contained a fixed proportion of larger grains ("porphyroclasts"). The matrix material (Brazil quartz) was the same in all experiments while two distinct types of porphyroclasts were used.

The quartz matrix comes from a dry Brazil single-crystal crushed in a stainless steel mortar. After crushing, we applied repeated cycles of sedimentation in a H_2O column to sort grains of a specific size. The powder we obtained consisted of grains with a diameter in the range of ~6-20µm, although a small fraction of the grains (~15% in volume), had larger, up to 110µm, diameter.

The first material chosen for the porphyroclast was dry Brazil quartz. A single euhedral crystal of ~4 cm long was cut, trying to avoid optically visible secondary fluid inclusions planes. Porphyroclasts were obtained by crushing the selected part of the crystal in a stainless steel mortar and separating a size in the range of 200-250 µm by sieving.

The second porphyroclast material was milky vein quartz from the Hyuga mélange, a low-grade metamorphic unit from the Shimanto Belt in Japan (Raimbourg et al., 2014; Palazzin et al., 2016 for detailed description). Fragments from mm-wide veins were crushed in an agate mortar and quartz was separated from the remaining matrix by a Frantz magnetic separator and density (Sodium Polytungstate) techniques. The material was sieved to separate the 200-250 µm size fraction. A final hand-picking was carried out to avoid possible clay mineral contamination.

The matrix and porphyroclasts were dried at 110°C for 48 hours before preparing the mixture. Four experimental samples were prepared by mixing 30% and 70% porphyroclasts of either Hyuga or Brazil quartz with the pure Brazil quartz matrix. In addition, one sample with 100% pure Brazil matrix was deformed.

To ensure an homogenous distribution of clasts in the matrix, we added acetone to the clasts+matrix mixture in a glass beaker and stirred the slurry obtained in an ultrasonic bath, until complete acetone evaporation (cf. de Ronde et al. (2005). The porphyroclasts and matrix quartz mixtures were dried at 110°C and then placed on the lower Al_2O_3-piston surface after adding distilled water with a micropipette. The material was wrapped in Ni-foil inside the Pt-jacket. The amount of water was adjusted to the proportion of the matrix (100, 70 or 30%), corresponding to an H_2O-content of 0.15 wt.% for matrix (**Table 1**). The second pre-cut piston was placed on top of the sample, and the Pt jacket was welded with a Lambert precision point welder. The sample was then placed in the center of a graphite furnace inside the solid confining medium (NaCl). The sample-piston assembly is illustrated in **Figure 1a**.

Pumping and heating were performed slowly to reach the desired temperature and pressure conditions (normally over ~9 hours). Confining pressure was initially increased to 150 MPa before heating. Temperature was increased in steps of 100°C at a rate of 25°C per minute at pressure intervals of several hundreds of MPa. When pressure and temperature were at 1.5 GPa and 800°C, axial piston movement was started at a constant displacement rate. The typical time to reach the hit point was ~20 to 24 hrs. During this stage, the sample was effectively subjected to hot isostatic pressing, leading to a denser aggregate.

The hit point, marked by a sharp increase in axial force, corresponds to the onset of sample loading and deformation. Axial force then rises rapidly to a maximum value (“peak stress”). The subsequent deformation of the sample, up to γ ~4-6, is achieved for near constant, or slowly decreasing axial force.

At the end of each experiment, the sample was quenched to a temperature of 200°C within 3 minutes. Subsequently, the confining pressure was lowered to room pressure over a period of several hours, keeping a differential stress of (initially) 100-200 MPa on the sample in order to minimize unloading cracks.

Some samples were kept under hydrostatic conditions without deformation to obtain information of the microstructures during the initial steps of the experiments. All samples were cut along their long axis normal to the shear zone in order to provide thin and thick sections for microscopy and FTIR analysis, respectively.

2.2 FTIR measurements

To enable analysis of the H_2O-content, slices of the single Brazil quartz crystal (cut in the direction normal to the [c]-axis) and isolated porphyroclasts of Hyuga quartz (both corresponding to the starting material) were firstly embedded in orthodontic acrylic resin (Vertex Orthoplast) and then manually doubly polished (thickness 120-140 µm). Deformed samples were cutted and directly polished to 120-140 µm_thick sections. Samples were then accurately cleaned in ultrasonic bath with acetone to remove remaining resin. The H_2O-content was determined by Fourier Transform Infrared (FTIR) spectroscopy with a microscopic FTIR continuum spectrometer (Nicolet-6700, Thermo Scientific) at the Institut des Sciences de la Terre d'Orléans (France). All the measurements were carried out at atmospheric temperature, after purging the optical path of the IR beam with dry air in order to avoid measurement of atmospheric water. A sodium chloride window was used to collect and subtract the background for each measurement. A 50×50 µm aperture window was used for all the analyses. 256 scans per spectrum were collected with 4 cm^{-1} resolution. We estimated the concentration of "molecular" H_2O, using the Paterson (1982) calibration of the integral absorption band between ~2800 and 3780 cm^{-1} using the Beer-Lambert law,

$$A= C * t * □$$

where *C* is the concentration, *t* the thickness, and □ the integrated molar absorption coefficient (0,8120 L cm^{-2} mol^{-1}). Sample thicknesses *t* was obtained from the height of the peak at 1790 cm^{-1} corresponding to the Si–O band, again making use of the Beer-Lambert law (e.g., Ito and Nakashima, 2002). H_2O concentration (wt. ppm H_2O/SiO_2) was obtained (**Table 1**) by dividing the H/10^6Si-value of the Paterson (1982) calibration by a factor 6.67 given in Kilian et al. (2016).

2.3 EBSD - CIP - Grain Size determinations

Crystallographic preferred orientation (CPO) of quartz was measured by electron backscatter diffraction (EBSD) (Lloyd and Freeman, 1994; Prior et al., 1999) and by computer integrated polarized (CIP) microscopy (Heilbronner and Barrett, 2014). EBSD patterns were acquired with an Oxford AZTEC system and a Nordlys detector on a FE- Zeiss Merlin compact SEM at the University of Tromsø. We used thin sections with a thin carbon coat at 70° tilt angle, 20 kV acceleration voltage, ~10 nA beam current, and 11 to 14 mm working distances at a step size of 0.1 µm. Initial noise reduction was performed with CHANNEL 5 software by removing isolated points and replacing non-indexed points with the orientation of their neighbors (interactively filled starting with eight similar neighbors down to six or five similar neighbors). Thin sections were rotated 45° counterclockwise in order to align shear zone boundaries (forcing block interface) to reference frame direction. Data were analyzed with MTEX toolbox (Hielscher and Schaeben, 2008). Analysis of the grain boundary fraction was carried out using EBSD maps. Grains were segmented based on c-axis misorientation after converting EBSD images to CIP images using a procedure described in Heilbronner and Kilian (2017).

3. RESULTS

3.1 Characterization of the starting material

Hyuga quartz has a milky appearance due to the great abundance of many tiny fluid inclusions (Palazzin et al., 2016). These inclusions range from a few to 10µm in diameter (Raimbourg et al., 2015) and are heterogeneously distributed in the porphyroclasts which look dark in thin section and grain mounts (**Figure 1b-1)**. As shown by FTIR spectra**,** OH content is variable as a consequence of the distribution of fluid inclusions (**Figure 1b-1)**. Mean measured values (listed in **Table 1)** are of the order of ~23,000 H/10^6Si, or ~0.34wt% H_2O, which is about twice the amount of H_2O added to the sample matrix. After the rise in T and P up to 800°C

and 1.5GPa, Hyuga porphyroclasts show a lower abundance of fluid inclusions than the starting material, so that they appear clearer (**Figure 1b-2**). The measured amount of OH is lowered to about half of the initial quantity (~12,000 H/10^6Si), corresponding to ~0.18wt%, similar to the added H_2O content of 0.15wt% (**Table 1**, **Figure 1b-2**).

Porphyroclasts of dry Brazil quartz are optically strain free and contain no fluid inclusions (**Figure 1b-3)**. The mean measured H content in Brazil quartz is about 260 H/10^6Si and confirms that this material can be considered as "dry" quartz for deformation (**Table 1**; Post and Tullis, 1998; Paterson, 1989)**.**

3.2 Mechanical data

Moderate peak shear stress and lower flow strength values (**Figure 2, Table 2**) indicate dominant plastic deformation in most samples at the applied strain rate of ~2.1 x 10^{-5} s^{-1}. Only the 70% Brazil clast sample reaches peak stress above the Goetze criterion ($\Delta\sigma$ = 1600 MPa at gamma ~2; **Figure 2**) for plastic deformation ($\Delta\sigma \approx P_{conf}$; Kohlstedt et al., 1995), all other samples are in the fully plastic regime. All curves are characterized by a first stage of a rapid increase in stress up to peak values (γ = 0 to ~0.5/1.5), followed by a weakening stage that may or may not reach steady state stress values.

Two samples with 100% matrix show a ~50% difference in peak stress (at γ ~0.8) and a smaller difference at γ ~3.5 (**Figure 2**). The sample with 30% Hyuga porphyroclasts shows a peak shear stress between that of the two matrix samples (**Figure 2**) and a final stress value that is almost identical to that of the matrix sample (~260 MPa) at gamma~3.2. The sample with 70% Hyuga porphyroclasts shows a considerably higher peak stress but weakens to a similar finite strength as the 30% Hyuga and matrix samples.

Samples with Brazil porphyroclasts reach higher peak shear stresses than their Hyuga porphyroclast counterparts: up to ~650 MPa for 70% clasts and ~420 MPa for 30% Brazil clasts. After the peak stress, all matrix + clast assemblages display significant weakening with a similar slope, irrespective of the nature of the clasts. It is remarkable that the flow stresses of three assemblages, containing 70% and 30% of Hyuga porphyroclasts and 30% of Brazil porphyroclasts, converge towards a common flow stress of ~250-280 MPa at γ ~3.3 (**Figure 2**), similar to the 100% matrix, regardless of their peak stress values.

3.3 Microstructural observations

3.3.1 Hot pressed material

After hot-pressing, only little porosity is observed, typically at triple junctions of grains (**Figure 3**). Pores rarely exceed 1µ diameter, and total porosity is estimated to be ~ 2 to 4 % of the sample volume. Very few open grain boundaries are present, but these are approximately normal to the piston axis, so that they probably result from quenching and unloading (**Figure 3**).

3.3.2 Pure matrix deformation

The deformed samples with pure 100% matrix are characterized by pervasive recrystallization of the deformed parts of the samples. Strain is partitioned into narrow regions at the piston ends, extending into a broader region, which occupies almost the full width of the shear zone in the center (**Figure 1a**). The quartz grains in the regions of strain localization show a strong shape fabric, and individual grain boundaries are difficult to detect in the high strain regions in the light microscope because of their strong CPO (see paragraph 3.5.1).

3.3.3 Matrix + Brazil porphyroclasts

In these samples, a foliation results from the elongation of matrix domains and recrystallized regions extending from porphyroclasts at an angle of about 18° to the shear zone boundaries (piston interfaces; **Figure 4a,b**). In the sample with 70% clasts, tails of recrystallized quartz (**Figure 4b,d**) extending from porphyroclasts define σ-type clasts (Hanmer, 1984b; Passchier and Simpson, 1986). Porphyroclasts in the assembly with 30% clasts show a variable shape: some are elongated, while others have an equant shape, both of which are mainly inherited from their pre-deformation state (**Figure 4a,c)**. Porphyroclasts contain few or no subgrains. Their rims are commonly sutured and their cores are surrounded by small recrystallized grains (**Figure 4c,d**). Some undulatory extinction and deformation lamellae are common **(Figure 5a,b).** These microstructures are characteristic of dislocation creep regime 1 described by Hirth and Tullis (1992). In both Brazil clast samples the extent of recrystallization of porphyroclasts is limited, and relict clasts and recrystallized rims are easy to distinguish (**Figure 4-5a,b**).

3.3.4 Matrix + Hyuga porphyroclasts

Hyuga porphyroclasts (6**a,b**) invariably are strongly elongated, up to an aspect ratio of ~10. Their shape fabric defines a foliation at about 10° to the shear zone boundaries. They are extensively recrystallized into elongated grain aggregates, with serrated boundaries, and subgrains, forming a microstructure of dislocation creep regime 2 of Hirth and Tullis (1992). Because of the penetrative recrystallization, former porphyroclasts are difficult to distinguish from the surrounding matrix (**Figs 5c,d and 6c)**, except for the fact that porphyroclasts recrystallized and grown into larger grains and subgrains than the matrix (**Figs 5c,d and 6c,d**). The clasts in the 70% Hyuga porphyroclasts sample are more pervasively recrystallized than in the 30% clast sample, possibly due to higher strain.

3.3.5 Shear Bands

In both samples containing Hyuga porphyroclasts, shear bands develop oblique to the shear zone boundaries in a synthetic orientation (c′-orientation) with the imposed shear sense (**Figs 6c,d and 7**). The angle between these planes and the shear zone boundary varies between ~25 and ~35°. The stretched porphyroclasts define the S-planes of a SC' fabric (C-planes are absent). Plane polarized light images show the shear bands as trails of small fluid inclusions (**Figure 7a**). The shear bands are most ubiquitous in the sample containing 70% of Hyuga porphyroclasts, where the bands cut across the matrix and the stretched porphyroclasts, making an average angle of 27 degrees with porphyroclast long axes. SEM images (**Figure**

7c) show that the C' bands are zones of high porosity, composed of cube-shaped, idiomorphic grains, of size ~2-5 µm, surrounded by voids.

3.4 H_2O content/distribution

3.4.1 Matrix

The original Brazil quartz crystal, from which the matrix was produced, contains a very low proportion of H_2O, of the order of ~250 H/10^6Si (**Table 1 and Figure 1b-3)**. In each experiment, H_2O had been initially added to the dry Brazil quartz matrix, with a proportion of 0.15wt%, or equivalently 10 000 H/10^6Si.

After the experiments, the matrix displays a broad absorption band in the region between 3000 and 3800 cm^{-1} (**Figure 8a**), representing the molecular H_2O in quartz and in the grain boundaries. From this broad absorption band, the H_2O content after experiments can be estimated as ~900 to 2900 H/10^6Si in deformed samples and ~4200 H/10^6Si in an undeformed sample (464GP, **Table 1**). The water initially added has been retained to variable extent in the matrix during the application of pressure and temperature and later deformation.

The same initial material (Brazil quartz matrix + 30% Hyuga porphyroclasts) was brought to high P and T in one experiment and then retrieved (464GP). In another experiment it was deformed to high strain (428GP). The Brazil matrix in the deformed sample contains ~1500 H/10^6Si, i.e. 2 to 3 times less than the corresponding experiment without deformation (~4200 H/10^6Si; **Table 1**).

Comparing the different experimental materials, the H_2O content of the matrix is significantly higher for experiments containing initially "wet" Hyuga porphyroclasts (~1500 for 30% and ~2900 H/10^6Si for 70% porphyroclasts) than in experiments containing initially "dry" Brazil porphyroclasts (~950 and ~1300 H/10^6Si for 30% and 70% of porphyroclasts) or experiments with 100% matrix (~800 H/10^6Si) (**Figure 8a, Table 1**). Additionally, in experiments containing Hyuga porphyroclasts, the H_2O -content of the quartz matrix and that of the recrystallized Hyuga clasts are similar after deformation, considering the large standard deviation: with 30% of clasts, the matrix contains ~1500 H/10^6Si and porphyroclasts ~2300 H/10^6Si, while for 70% clasts, the matrix contains ~2900 H/10^6Si and porphyroclasts ~2350 H/10^6Si (**Table 1**).

All spectra show discrete absorption bands at 3363, 3382, and 3595 cm^{-1}, which were not present in the original Brazil quartz spectra (cf. **Figures 1D and 8**). The most prominent discrete absorption band in the deformed matrix measurements is at 3595 cm^{-1}.

3.4.2 Porphyroclasts

Hyuga porphyroclasts display a broad absorption band in the region between 3000 and 3800 cm^{-1} (**Figures 1b,c,d and 10a**), which is related to molecular H_2O contained in the large number of fluid inclusions initially present. During hot pressing the broad band of molecular H_2O shows a general decrease with respect to the as-is material. This reduction in water content is enhanced with deformation, as Hyuga porphyroclasts in deformed samples contain ~1/10 of their initial water content (**Table 1, Figure 9a**).

In addition to this evolution of the H_2O content, the shape of the H_2O spectrum is also modified by the application of P-T conditions and deformation from a broad triangular absorption centered around around 3400cm^{-1} that is charateristic of fluid H_2O to a very broad flat flat shape absorption (**Figure 9a**) that is unlike absorption spectra of liquid H_2O. The position of discrete absorption bands, related to structurally-bound H_2O, are also modified. The initial spectrum displays only a discrete absorption band at 3382 cm^{-1}. Application of P-T condition results in the development of a band at 3585cm^{-1}, while after deformation a discrete band around 3595cm^{-1} appears as well. As a result of this evolution in shape and integrated area, recrystallized Hyuga porphyroclasts and the fine grained matrix converge towards a similar IR spectrum (**Figure 9b**).

Initially, Brazil porphyroclasts contain virtually no H_2O (~250 $H/10^6Si$), resulting in a flat absorption spectrum (**Figure 8b**), where only one secondary absorption band at 3485 cm^{-1} is visible. The application of P-T conditions and deformation **(Figure 10, Table 1)** results first in the increase in H_2O content in the cores of the porphyroclasts (~650 $H/10^6Si$) and in their recrystallized rims (~1500 for 30% and ~900 $H/10^6Si$ for 70% of porphyroclasts). The very weakly deformed cores, showing only undulatory extinction, contain a smaller amount of H_2O (**Figure 10b,c,f**) than observed for the recrystallized regions with their grain boundaries (**Figure 10d,e,f**). Furthermore, new discrete absorption bands appear at 3595 cm^{-1} and at 3363 cm^{-1} in the recrystallized region, whereas the core shows a discrete band at 3585 cm^{-1}, which is absent in the recrystallized region (**Figure 10a,f**).

3.4.3 Shear bands

In the experimental sample containing 30% of Hyuga porphyroclasts, the shear bands that cut across porphyroclasts and matrix contain a high H_2O concentration of ~3700 $H/10^6Si$ (**Table 1**). This H_2O content is significantly higher than either porphyroclasts (~2300 $H/10^6Si$) or the matrix (~1500 $H/10^6Si$) that hosts these bands. It corresponds to trails of fluid inclusions (optical observations) and the presence of abundant voids (SEM observations) along the shear bands (**Figure 7a,c**).

3.5 Crystallographic fabrics

Grain boundary maps, orientation images and pole figures are derived from EBSD maps and shown for a pure matrix sample and for one sample containing 70% Hyuga and one with 70% Brazil clasts. For easier interpretation, the orientation images are recalculated as c-axis orientation images (see color look-up table on the right of **Figs 11b-12b and 13b**).

3.5.1 100% Matrix

In the 100% matrix experiment, the central region of pervasive recrystallization of the sample shows elongated grains, whose long axes are oriented at ~25 degrees (on average) from the shear plane (**Figure 11a,b**). Their CPO shows a well-defined maximum rotated synthetically with the sense of shear, and all crystallographic axes are concentrated in or near the X-Z plane (**Figure 11c**).

3.5.2 Recrystallized Hyuga porphyroclasts CPO

EBSD map shows that a large proportion of initial Hyuga porphyroclasts, strongly elongated after deformation, consists of recrystallized grains with small grain size (light blue domain, **Figure 12a,b**).

The CPO shows a similar asymmetry with respect to the shear plane as the 100% matrix. Parts of the recrystallized regions show many subgrain boundaries in a rather uniform CPO domain (**Figure 12b**).

3.5.3 Recrystallized tail of a Brazil porphyroclast

In the experiment with 70% Brazil quartz, the crystallographic fabric of the recrystallized tail is qualitatively similar as that of the 100% matrix, but the grain size distribution is broader (**Figure 13a,b**). The c-axis maxima are slightly weaker (**Figure 13c**). The recrystallized tail appears to have a better developed CPO than the matrix (orange domain, **Figure 13b**).

3.5.3 Shear bands and strain shadows

Shear bands are developed only in Hyuga clast samples. CIP analysis of these samples reveals that shear bands inside larger porphyroclasts have a completely different c-axis orientation from that of the surrounding material, as seen in light microscope images with the compensation plate inserted (**Figure 7b)**. Strain shadows around Brazil porphyroclasts constitute other high-porosity domains where small idiomorphic grains are surrounded by voids, and the crystallographic orientation of these small grains, similar to that of shear bands, is very different from surrounding quartz. The strong contrast in orientation between the grains in shear bands and pressure shadows and the surrounding material, the high-porosity, and the grain shapes suggest that these grains formed as a result of precipitation in a fluid filled porosity.

4. DISCUSSION

4.1 Mechanical Data

After exhibiting an initial peak stress, all samples deform at flow stresses well below the values of the confining pressure (**Figure 2**; Goetze Criterion: Kohlstedt et al., 1995). The inference of the Goetze Criterion that fractures opening and extension are suppressed when Pc > differential stress is consistent with the fact that non of our sample contained thoroughgoing fractures. The 100% Brazil quartz matrix samples show a higher flow stress than that of wet polycrystalline quartz of Hirth and Tullis (1992) in coaxial experiments at the same temperature and confining pressure. The shear strain rate of our experiments is faster than the coaxial strain rate of Hirth and Tullis (1992), which may explain the differences. From the mechanical data it is clear that the originally dry Brazil quartz matrix material has become fully "wet" during pressurization and heating, as it has been achieved in experiments previously by Post and Tullis (1998) and Rutter and Brodie (2004a).

All samples with porphyroclasts show a pronounced peak stress and subsequent weakening behavior, consistent with a higher initial strength of the large porphyroclasts, which subsequently weaken during recrystallization. Even the Hyuga quartz, which contains a lot of H_2O in the form of aqueous fluid inclusions and thus may be expected to be weaker than the pure Brazil quartz matrix, shows this behavior. The mechanical evolution of the sample raises two points: (1) Porphyroclast material shows pronounced strain weakening, probably caused by recrystallization (2) Fine grained quartz material tends to be weaker than that with coarse grained porphyroclasts. The former point has already been addressed by Hirth and Tullis (1992), who have observed strain weakening behavior for dislocation creep regime 1. The weakening is attributed to local grain boundary migration (bulging recrystallization) of more or less undeformed porphyroclasts. In our examples here, dynamic recrystallization takes place by progressive subgrain rotation (see below), so that the recrystallization mechanism does not seem to be the only controlling factor for the weakening.

Steady state is reached by the 30% Hyuga material (428GP) after $\gamma \approx 1.5$ (**Figure 2**). The 70% Hyuga sample (456GP) reaches similar stresses as the 30% sample, but at higher gamma values and after higher peak stress. The grain sizes of the 70% Hyuga sample are smaller, even though the finite stress values of the samples are identical. The findings are consistent with the results by Kidder et al. (2016), who find that the recrystallized grain size is dependent on stress history.

Samples with dry Brazil porphyroclast samples do not reach steady state after $\gamma = 3.5$ or 4 is consistent with Brazil clasts behaving as more rigid particles, and their recrystallization takes more strain than does recrystallization of the Hyuga clasts. The high peak strength of the 70% Brazil clasts sample can be attributed to the high strength of the Brazil clasts themselves with low H_2O content. The fact that they survive deformation as more or less rigid particles implies that they have not become sufficiently hydrated. Only limited recrystallization takes place at their margins, where tails of recrystallized quartz grains develop (**Figs. 5-6a,b and 14**). The CPO of their recrystallized grains is oriented synthetically with respect to the imposed shear sense (dextral; **Figure 14**), i.e. similar to that of weaker material of other samples.

Applying the empirical quartz flow law by Hirth et al. (2001), and the Paterson & Luan (1990) flow law (for silicic acid), we estimated the differential stress of our quartz matrix for strain rate values of $2*10^{-5}s^{-1}$. Both flow laws predict lower shear stresses ($\Delta\sigma/2$) than our experimental values for pure matrix (111 MPa and 178 MPa versus observed ~200 MPa) but the values are not far off (yellow star and red dot in **Figure 2**).

4.2 Effect of H_2O on deformation

Our samples are deformed by crystal-plastic processes, so that they can be compared with the different deformation regime defined in Hirth and Tullis (1992). Even though Brazil and Hyuga porphyroclasts were deformed at the same P and T, the degree and mechanism of recrystallization was quite different in the two materials.

Dry Brazil porphyroclasts show undulatory extinction and abundant deformation lamellae as typical features for dislocation glide with limited recovery or recrystallization in quartz. These features usually occur together with small scale fractures, kinks or short wavelength misorientation bands, and dislocation tangles (Hirth and Tullis, 1992, Trepmann and Stoeckhert, 2013, Stunitz et al., 2017) and can be compared to microstructures observed in the dislocation creep regime 1 of Hirth and Tullis (1992). The presence of small recrystallized grains limited to prophyroclasts rims suggests the onset of subgrain rotation recrystallization. Recrystallized tails at porphyroclasts form a CPO similar to the matrix CPO (**Figure 13**), consistent with activation of slip on the basal <a> system (Schmidt and Casey, 1986; Law, 1990).

Deformed milky Hyuga quartz shows very different microstructures. The shape of highly elongated Hyuga porphyroclasts can be compared with natural quartz aggregates deformed at mid-greenschist conditions (Law, 1984) or with experimentally deformed Black Hill Quarzite (BHQ) described in regime 2 by Hirth and Tullis (1992) or by Hirth et al., (2001). These elongated grain aggregates are recrystallized to a great extent (**Figs. 6 and 12**). Similar microstructures, and corresponding activated slip systems, are reported also for BHQ (Heilbronner and Tullis, 2006) deformed at higher temperatures and higher strain rates. According to our microstructural observations and CPO, recrystallization took place by subgrain rotation. The development of a common CPO for recrystallized porphyroclasts and matrix indicates that deformation is rather homogenously accommodated within the whole system and dominated by basal <a> slip.

The difference between Brazil porphyroclasts, deforming with limited recrystallization, and Hyuga porphyroclasts, pervasively recrystallized by subgrain rotation, can only be explained by their original difference in H_2O content. Our observations further support the effect of H_2O on enhancing microstructural development and recrystallization proposed by Jaoul et al. (1984), Tullis and Yund (1989) and Hirth and Tullis (1992).

Most samples converge to a similar strength after a shear strain of ~3 and recrystallization of large volume fractions of the samples (**Figure 2**), even though the initial concentrations of H_2O differed (**Figs. 9 and 11, Table 1**). Some of the main parameters controlling strength are therefore grain size and H_2O distribution, and we can deduce that weakening in experiments with Hyuga porphyroclasts is due to grain size reduction and fluid redistribution as a consequence of dynamic recrystallization.

4.3 Evolution of H_2O with deformation

4.3.1 H_2O speciation

In addition to the "broad" band of molecular H_2O in the range 2800-3800 cm^{-1}, our samples show a large set of secondary, discrete absorption bands distributed between 3660 and 3300 cm^{-1} (**Figs 8-9 and 10 and Table 3**). Most of these bands were not present in the original material and appear after deformation.

4.3.1.1 – Absorption band at 3595 cm^{-1}.

The band 3595 cm^{-1} has been detected in different kinds of natural clear quartz and natural/synthetic amethyst (e.g. (Kats, 1962; Aines and Rossman, 1984; Rovetta, 1989; Kronenberg, 1994), and in natural deformed and then annealed quartzite (Niimi et al., 1999). The common interpretation is that H^+ charge compensates for Al^{3+} substituting for Si^{4+}. Gleason and DeSisto (2008) described this band in pegmatitic quartz and quartz ribbons, giving the same interpretation.

In our experiments, the band at 3595 cm^{-1} is not detected in all samples but it is strictly correlated with attaining P and T and most importantly with deformation. This band is first identified in all matrix analyses (**Figure 8a**), while it is absent in the IR spectra of undeformed Brazil quartz (**Figure 8b**). In Hyuga porphyroclasts, it is not observed at hot-pressed conditions, but it develops after deformation, when porphyroclasts are pervasively recrystallized (**Figure 9**. The band is also observed in Brazil porphyroclasts, but exclusively in their recrystallized tail (**Figure 10b,f**). The 3595 cm^{-1} band is therefore closely associated with recrystallized aggregates of grains, suggesting that the OH species of this band are associated with grain or perhaps subgrain boundaries.

Several studies on quartz IR spectra in naturally-deformed rocks further substantiate the connection between a discrete absorption band near 3600 cm^{-1} and recrystallization microstructures. Quartz in mylonites from Sambagawa metamorphic rocks in Japan (Nakashima et al., 1995) and the western Adirondack in the USA (Gleason and DeSisto, 2008) show a discrete absorption band around 3600 cm^{-1}. Such a peak is absent in other mylonites, such as granite mylonite in the vicinity of the Median Tectonic Line in Japan (Nakashima et al., 1995; Niimi et al., 1999). However, in these samples it is not clear whether grain boundaries were analyzed by FTIR in addition to grain interiors. The speciation of OH in quartz at subgrain/grain boundaries may be related to silanols at the quartz surface, although the corresponding absorption bands are reported at slightly higher wavenumbers (e.g. 3627 and 3649 cm-1, see the review in (Kronenberg, 1994)) than the ~3595 cm^{-1} peak observed in our study. In summary, a strong connection between increased surface area by recrystallization microstructure and 3595 cm^{-1} absorption band is clear from this study, but the nature of this OH absorption band requires further work.

4.3.1.2 – Absorption band at 3585 cm^{-1}

The absorption band at 3585 cm^{-1} exists in both, Hyuga and Brazil porphyroclasts after deformation (**Figs. 9a,b and 10**). This band has been observed in different materials as amethyst (Kronenberg, 1994, Chakraborty and Lehmann 1976), metamorphic cherts (Ito and Nakashima, 2002), chalcedony (Frondel, 1982; Graetsch, 1985,1987), flint (Graetsch, 1987), agate (Yamagishii et al., 1997) and synthetic quartz (Stalder and Konzett, 2012) Wood, 1960, Kats, 1962; Aines and Rossman, 1984; Cordier and Doukhan, 1989; Chakraborty and Lehmann, 1976; Paterson, 1986; Rovetta, 1989). In experiments of hydrothermal growth of quartz, the intensity of the band increases with pressure and H_2O activity in the surrounding fluid phase (Stalder and Konzett, 2012). A connection of this 3585 cm^{-1} absorption band to deformation was established in deformation experiments (Stünitz et al., 2017), where the development of 3585 cm^{-1} band is confined to deformed parts of single quartz crystals. In addition, a band at 3580 cm^{-1} was observed to develop after annealing of quartz at high temperature (Cordier and Doukhan, 1991; Rovetta et al., 1986). In the latter set of experiments, it was correlated with the formation and healing of cracks during annealing, while no cracks were reported in the former study. Stünitz et al. (2017) suggest that the 3585 cm^{-1} band may record OH-defects associated with dislocations. The systematic association between this band and deformation microstructures is also apparent in our samples. This band, absent in “as-is” Hyuga milky quartz samples, appears after both, hot-pressing and deformation (**Figure 10a**), while in Brazil quartz it is observed only in unrecrystallized but deformed (e.g. lamellae) porphyroclasts cores (**Figure 10f**). This close connection to microstructures supports the conclusion by (Stünitz et al., 2017) that the band 3585 cm^{-1} is caused by structurally bond OH at dislocations.

4.3.1.3 – Absorption bands at 3382 cm^{-1} and at 3363 cm^{-1}:

The sharp absorption bands at 3382 cm^{-1} and at 3363 cm^{-1} are specific to the nature of the experimental material, either Hyuga or Brazil quartz.

The absorption band at ~3380 cm^{-1} is systematically observed in Hyuga milky quartz before and after deformation. It has been detected in quartz grains of gneiss (Gleason and DeSisto, 2008) and in cherts (Ito and Nakashima, 2002) and is attributed by several authors to OH groups bonded with Al^{+3} substituting for Si (Pankrath, 1991; Stalder and Konzett, 2012) Kronenberg, 1994; Suzuki and Nakashima, 1999; Gleason and DeSisto, 2008). This interpretation is supported in our case by the high content of aluminum in Hyuga quartz (Raimbourg et al., 2015).

The band at 3363 cm^{-1} is observed only in deformed and recrystallized Brazil quartz, either in the matrix (**Figure 9a**) or at recrystallized tails of porphyroclasts (e.g. **Figure 11**). While it is generally assigned to surface Si-OH groups (Yamagishi et al., 1997), our study does not yield further clues to this attribution.

To summarize, we infer that three different species of H_2O are observed after deformation. The first one is molecular H_2O incorporated in porphyroclasts on the form of fluid inclusions, represented by the broad absorption band between 2800 and 3800 cm^{-1}. The second type of H_2O is stored in grain boundaries as a result of recrystallization processes. It is represented by the discrete band at 3595 cm^{-1} corresponding to structurally bond OH-defects. The third type of H_2O is characterized by the discrete band at 3585 cm^{-1} and is probably due to OH-defects on dislocations.

4.3.2 Mechanisms of H_2O incorporation and expulsion

H_2O content in “as-is” Hyuga clasts is estimated at ~22,900 H/10^6Si. It decreases first with the application of temperature and pressure to ~12,000 H/10^6Si (hot-pressed conditions), and then further decrease to ~2,300 H/10^6Si after deformation of γ~4 (**Table 1 and figs. 1b,c,d and 10**). The expulsion of H_2O during the application of pressure and temperature does not proceed through recrystallization, as the corresponding new grains were not observed (**Figure 1c**). In the absence of significant deformation and formation of grain boundaries through recrystallization, the expulsion of H_2O is probably caused by micro-fractures draining fluids from inclusions. One driving force for fracturing during the rise in P and T conditions is the ΔP between the fluid pressure in the inclusions initially present (imposed by the fluid isochoric line) and the confining pressure (experimentally imposed). Decrepitation of fluid inclusions is observed for relatively low ΔP of less than a couple of 100 MPa in experiments (Hall and Sterner, 1993; Vityk and Bodnar, 1995). Furthermore, the initial assembly has a relatively large porosity and heterogeneous grain size distribution (clast + matrix). The application of P and T results in compaction, hence in local stress concentration, which may result in fracturing that may drain fluid inclusions. These fractures are not easily observable because they are systematically healed at high pressure and temperature (Tarantola et al., 2010).

During subsequent plastic deformation, dynamic recrystallization (**Figs. 6-7-13**) involving formation and mobility of grain boundaries, provides an efficient process to further decrease the H_2O concentration in the quartz porphyroclasts (**Figure 14a**). Grain boundary mobility has an important effect on modification of volume and distribution of fluid inclusions in experiments (Olgaard et FitzGerald, 1993; Schmatz et Urai, 2010). Observations in natural samples (e.g. Kilian et al., 2016) are consistent with experimental ones. In domains where the Hyuga quartz recrystallized in nature as a result of deformation, the number of fluid inclusions, hence the H_2O content, is strongly decreased (Palazzin et al., 2016). Similarly, Ito and Nakashima (2002) show a strong decrease in the total H_2O content with increasing recrystallization. This implies that extensively recrystallized "dry" porphyroclasts in natural shear zones might have been initially wet.

In contrast to Hyuga porphyroclasts, "as-is" Brazil porphyroclasts have a very low initial H_2O content (~260 H/10^6Si). After deformation, both, slightly deformed cores and strongly recrystallized domains, show a significant increase in H_2O: up to 640 and 950-1530 H/10^6Si, respectively (**Table 1**, **Figures 11-14a**). Their final content is similar to the hydrated matrix, which indicates a transfer of H_2O from the matrix to the porphyroclasts during deformation.

The process responsible for the increased H_2O content of recrystallized tails of Brazil porphyroclasts is probably identical to that of Hyuga clasts inferred above. The transfer of H_2O to the unrecrystallized cores of Brazil porphyroclasts is probably caused by microcracking as inferred by Kronenberg et al., (1986); Rovetta et al., (1986); Gerretsen et al., (1989) and Cordier and Doukhan (1989, 1991). The H_2O uptake by non-recrystallized cores of Brazil porphyroclasts, has a limited weakening effect, as attested by the higher strength of samples with a high content of Brazil porphyroclasts (**Figure 2**). Their final H_2O content, ~640H/10^6 Si, is nevertheless higher than the minimum amount of H_2O in wet synthetic quartz (~200 H/10^6 Si) necessary for weakening of these crystals (Kekulawala et al., 1978, 1981).

4.3.3 H_2O budget

4.3.3.1 Concentration and distribution of H_2O

We measured relatively large and variable (from ~810 to ~3710 H/10^6Si) concentrations of H_2O in the deformed quartz assemblies (**Table 1**). The large variability reflects first the difference in initial H_2O content: in deformation experiments with Hyuga porphyroclasts, the final H_2O content is between ~1470 and 3710 H/10^6Si, while in experiments with Brazil porphyroclasts, or pure matrix, the final H_2O content is between ~640 and 1530 H/10^6Si. Hyuga porphyroclasts, with their stored high H_2O content in fluid inclusions, act as an additional source of H_2O.

The experiments were carried out to large shear strain in an attempt to reach some steady-state of the microstructure and H_2O concentration. The flat portions of σ-□ curves do not reach perfect steady-state, but the convergence of strengths of most samples indicates that some final stage of the microstructural development has been reached. In order to find a physical meaning of the H_2O concentration in experiments with Hyuga porphyroclasts, we need to consider where the H_2O is stored, as the IR analysis window size (50x50µm) is larger than the grain size, so that the analyses include grain interiors and grain boundaries.

In experiments in quartzite of a large grain size, carried out at the same P-T conditions as ours, a strain rate of $10^{-6}s^{-1}$ and with 0.3 wt% H_2O (Post and Tullis, 1998), the H_2O content in quartz interiors is ~800 $H/10^6Si$, i.e. considerably lower than that in the finely recrystallized Hyuga material, in spite of the very large amount of initially added H_2O (0.3 wt% $H_2O \approx$ 20,000$H/10^6Si$). In natural mylonite deformed at 800°C and 800MPa, the intracrystalline H_2O content is ~320 $H/10^6Si$ (Gleason and DeSisto, 2008)). A compilation of data of natural quartz deformed in nature and in experiments, shows that intragranular H_2O is significantly lower than bulk measurements, which include the contribution of H_2O at grain boundaries (Kilian et al., 2016). This hypothesis is supported by direct FTIR transects across grains and their boundaries (Post and Tullis, 1998), or by the inverse relationship, in various metamorphic rocks, between the grain size of a rock and the H_2O volume that can be stored in the grain aggregate (Ito and Nakashima, 2002).

The concentration of H_2O stored in the grain boundaries of the recrystallized material varies systematically; in experiments with 30% or 70% of Hyuga porphyroclasts, the recrystallized porphyroclasts yield an approximately uniform content of ~2300 $H/10^6Si$. The matrix contains similar amounts of H_2O (~1500 and 2900 $H/10^6Si$). These matrix H_2O contents are systematically larger than in the 100% matrix experiment (~800 $H/10^6Si$), despite the same amount of initially matrix-added water. Thus, H_2O is redistributed from Hyuga porphyroclasts to the matrix producing a uniform range of H_2O contents in Hyuga porphyroclasts and matrix. The H_2O concentration tends to some "equilibrium" concentration, similar to the microstructural evolution which tends to some final "equilibrium" state (**Figure 14a**).

4.3.3.2 Shear bands: evidence for excess H_2O

Shear bands are primarily observed in experiments with Hyuga porphyroclasts and are composed of small faceted quartz grains surrounded by void space (**Figure 7c**). IR measurements show that they contain a significantly larger amount of H_2O than the surrounding matrix (**Table 1**). Their CPO is also different from the surrounding quartz matrix (**Figure 12**). The grain shapes, presence of voids between crystals, and the different crystal orientations from host quartz suggest growth of these quartz grains in a pore space filled with fluid during deformation at high P and T. These shear bands appear to be the locations where excess free fluid phase is stored.

4.3.4 H_2O stored in the grain boundary region

We observed that the deformed quartz aggregates develop towards a common microstructure (**Figs. 11-12 and 13**), strength (**Figure 2**), and H_2O content of the matrix, clasts, and recrystallized material regardless of the initial starting material and relative clast contents (**Figure 14a**). The redistribution of H_2O mainly takes place by recrystallization and formation of new grain boundary area. If it is assumed that the largest part of the H_2O is distributed along the grain boundary regions (the grain interiors cannot store a large amount of H_2O as fluid inclusions because the grain size is below 10 µm), then the volume fraction of H_2O in the quartz aggregate can be plotted against the grain boundary area per analyzed volume (**Figure 14b**). The volume fraction of H_2O is measured by FTIR (**Table 1**), and the grain boundary density (length per surface) is determined by EBSD in the deformed microstructures (**Figs. 11-12 and 13, Table 4**). A similar approach was taken by (Ito and Nakashima, 2002), who used modeled average grain sizes instead of measured boundary fractions. As a result, the pure matrix and the matrix with Brazil clasts have the same nominal grain boundary widths of ~0.7 nm, whereas the matrix with Hyuga clasts has a grain boundary width which is more than twice this width (~1.7 nm; **Figure 14b**). Realistic grain boundary widths have been determined to be ~0.5 nm for feldspar (Hiraga et al., 2004) and ~1nm for pyroxene (Raimbourg et al., 2011), of similar magnitude to those determined here for quartz. The physical state of H_2O stored at grain boundaries is not established, nor the precise nature of the grain boundary itself (Raimbourg et al., 2011). Two types of models are usually proposed for H_2O along the grain boundary: (1) A thin molecular film or (2) A "channel-island" structure, where domains of thin film ("islands") are separated by channels where the thickness of H_2O is larger (e.g. (Den Brok, 1998; Nakashima, 1995)). Our results cannot resolve the details of H_2O distribution along grain boundary, and the method employed here is neither appropriate nor intended for an exact determination of a grain boundary width. The "nominal boundary width" obtained here is merely a measure of the H_2O storage in the grain boundary region under the assumption that the H_2O is evenly distributed along the grain boundaries with a common grain boundary width (**Figure 14a**).

The thicker nominal grain boundary width of the sample with Hyuga clasts and higher H_2O content coincides with the occurrence of shear bands (absent in other samples), which are sites of porosity and thus H_2O storage. It is likely that the nominal boundary width of ~1.7 nm corresponds to the H_2O storage capacity of the grain boundary region. If this storage capacity is exceeded, shear bands may develop. This process accounts for the fact that shear bands develop principally in the material with the highest initial H_2O content (i.e. in the samples with Hyuga porphyroclasts). Riedel shear bands, formed during deformation and acting as drains to collect the H_2O from the surrounding matrix, have been similarly described in wet (1.3 wt% H_2O) Dover flint experiments (Schmocker et al., 2003).

The shear bands do not have a weakening effect on the bulk sample: The sample with 70% Hyuga clasts and the highest H_2O content is not weaker than others (**Figure 2**). The lack of weakening by shear bands can be explained by a lack of simple connectivity of these bands on the sample scale (Pec et al., 2016; Marti et al., 2017).

If H_2O is principally stored at grain boundaries, the storage capacity of the grain aggregate is controlled by the grain size distribution and evolution. The process of redistribution of H_2O takes place by different processes of microcracking (including fluid inclusion decrepitation) and formation of grain boundaries by recrystallization. These processes can be observed in natural samples and the H_2O storage capacity will be an important parameter to be determined for deformation in natural samples, too.

5. Conclusions

In this experimental study the mechanical behavior, microstructural evolution, and H_2O content of different starting materials of "wet" quartz converge at higher shear strain at T=800°C, strain rate=$5*10^{-5}$ s^{-1} and Pc=1.5GPa. From these results we draw several conclusions:

- The high crystalline H_2O content, initially present in the form of fluid inclusions in wet quartz, is responsible for enhancing the recrystallization rate, in contrast to initially dry crystals that do not recrystallize extensively.
- Sharp absorption bands at 3585 cm^{-1} and 3595 cm^{-1} develop during deformation. The occurrence of the 3585 cm^{-1} band is consistent with dislocation-bound OH, whereas the 3595 cm^{-1} band most likely indicates OH adsorbed at grain boundaries.
- Recrystallization results in a clear decrease in H_2O concentration in quartz crystals initially rich in fluid inclusions, whereas H_2O uptake in initially dry crystals takes place by microcracking.
- In the deformed and recrystallized assemblies, most H_2O is stored in the grain boundary region. The amount that can be stored in the grain boundary (i.e. the storage capacity) is limited and corresponds to a nominally ~1.7 nm thick grain boundary

region. H_2O in excess of this nominal thickness is drained into micro-veins, formed as dilatant synthetic shear bands.

- These dilatant shear bands do not control the strength of samples as they are not simply connected.

Acknowledgements

We thank S. Janiec and G. Badin for thin and thick sections preparation, I. Di Carlo for help with the EBSD analyses, and S. Marti and B. Richter for their help in CIP and mechanical data processing. This work has received funding from (i) the European Research Council (ERC) under the seventh Framework Program of the European Union (ERC Advanced Grant, grant agreement No 290864, RHEOLITH) and (ii) the Labex VOLTAIRE (ANR-10-LABX-100-01), which are acknowledged. We gratefully thanks A. Kronenberg and L. Menegon for their very constructive reviews and the editor T. Takeshita for his help.

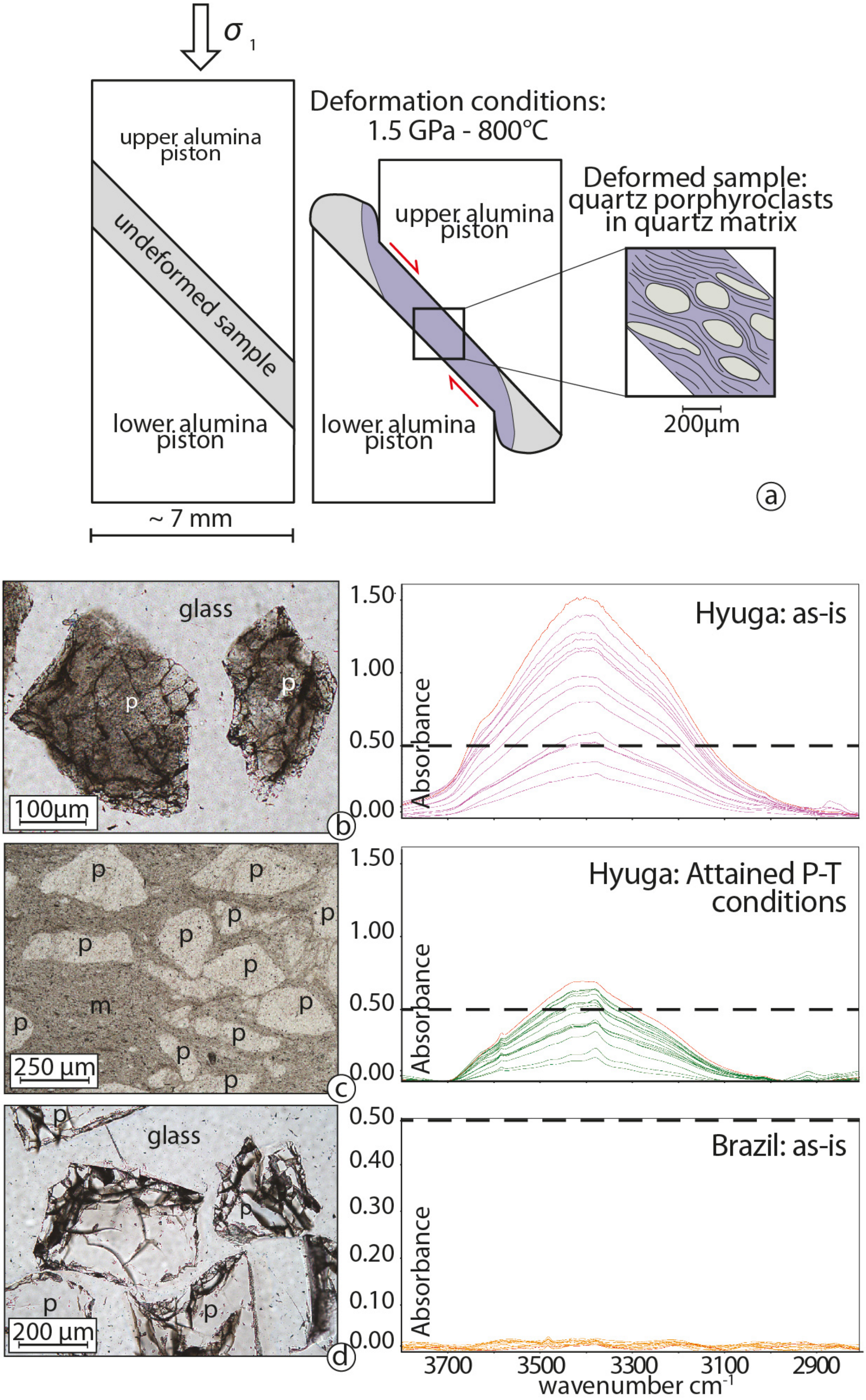
σ 1
upper alumina piston
undeformed sample
lower alumina piston
~ 7 mm
Deformation conditions:
1.5 GPa - 800°C
upper alumina piston
lower alumina piston
Deformed sample:
quartz porphyroclasts
in quartz matrix
200µm
a
glass
p
p
100µm
b
Hyuga: as-is
1.50
1.00
0.50
0.00
Absorbance
p
m
250 µm
c
Hyuga: Attained P-T conditions
1.50
1.00
0.50
0.00
Absorbance
glass
p
200 µm
d
Brazil: as-is
0.50
0.40
0.30
0.20
0.10
0.00
Absorbance
3700
3500
3300
3100
2900
wavenumber cm⁻¹

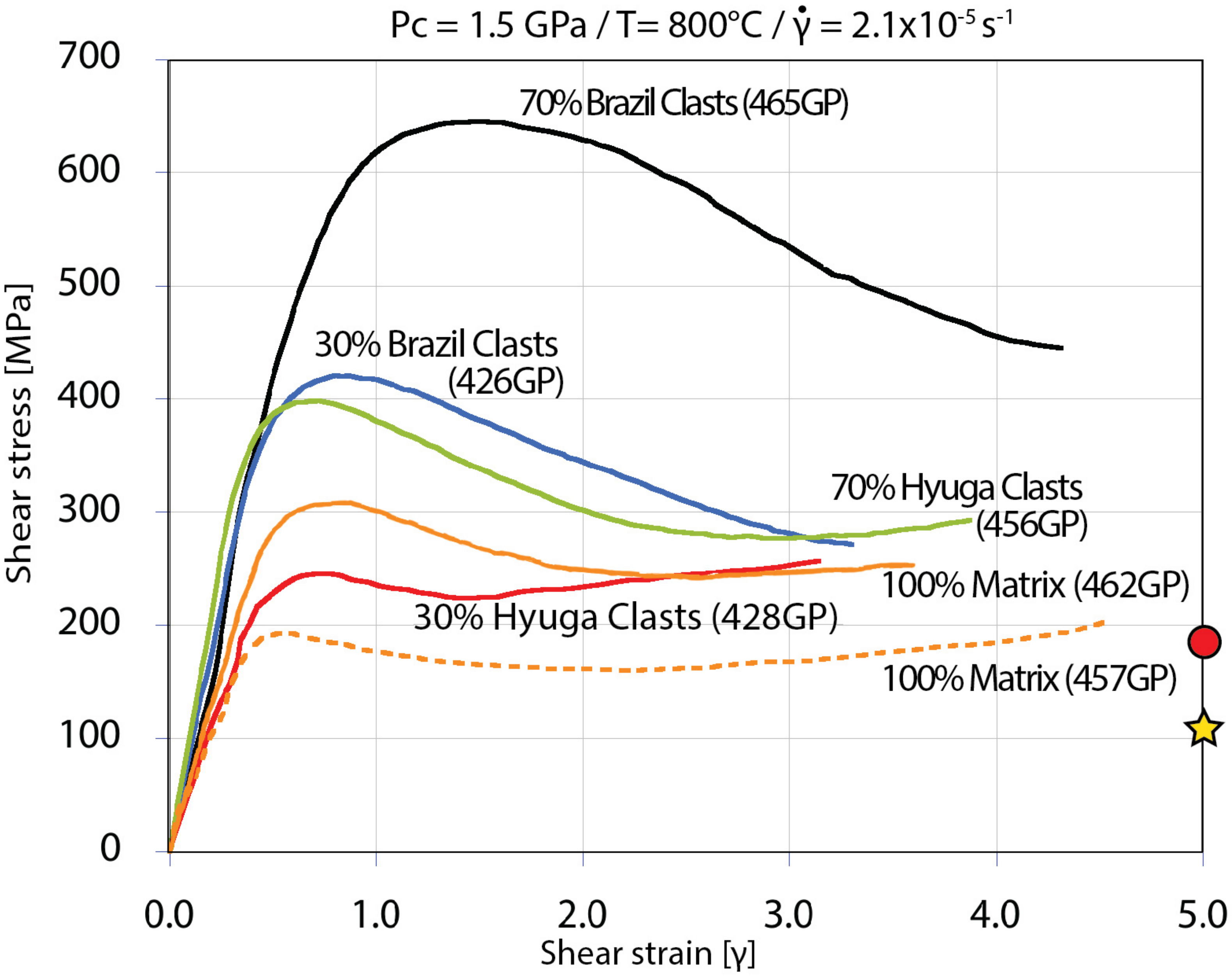

$Pc = 1.5$ GPa / $T = 800°C$ / $\dot{\gamma} = 2.1\times10^{-5}\ s^{-1}$
70% Brazil Clasts (465GP)
30% Brazil Clasts (426GP)
70% Hyuga Clasts (456GP)
100% Matrix (462GP)
30% Hyuga Clasts (428GP)
100% Matrix (457GP)
Shear stress [MPa]
Shear strain [γ]
0
100
200
300
400
500
600
700
0.0
1.0
2.0
3.0
4.0
5.0

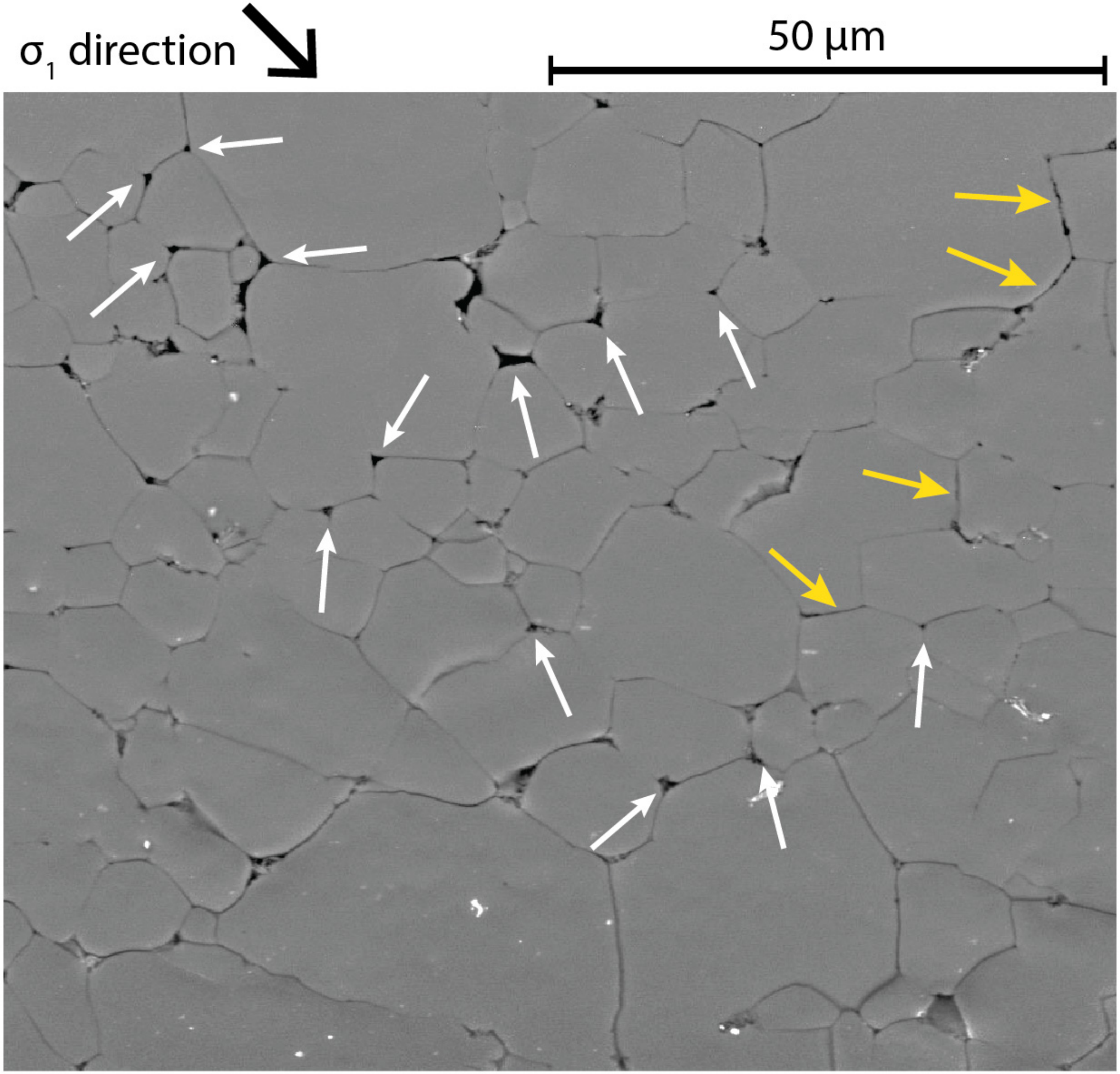
σ₁ direction
50 µm

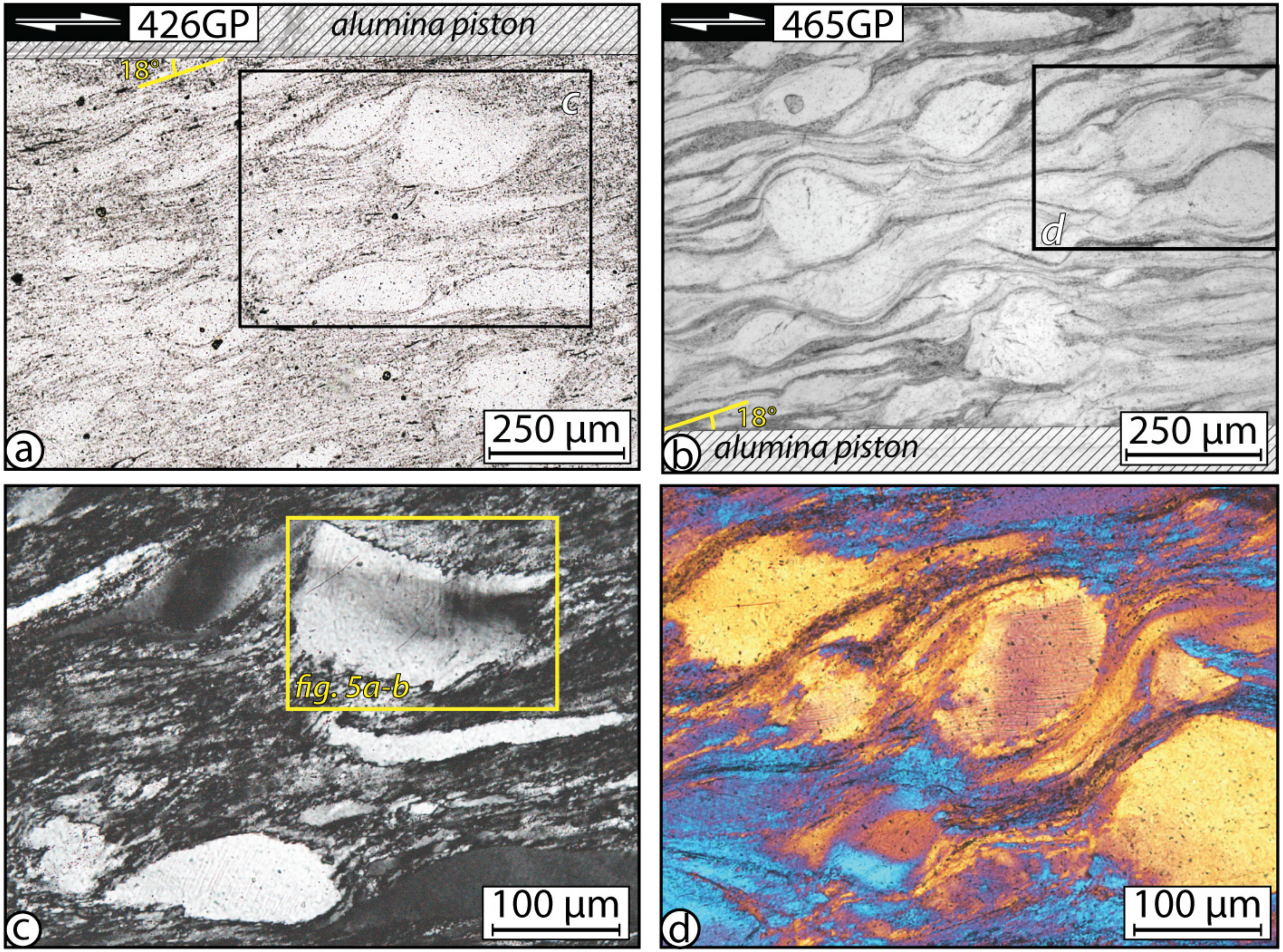

30 % BRAZIL porphyroclasts

70 % BRAZIL porphyroclasts

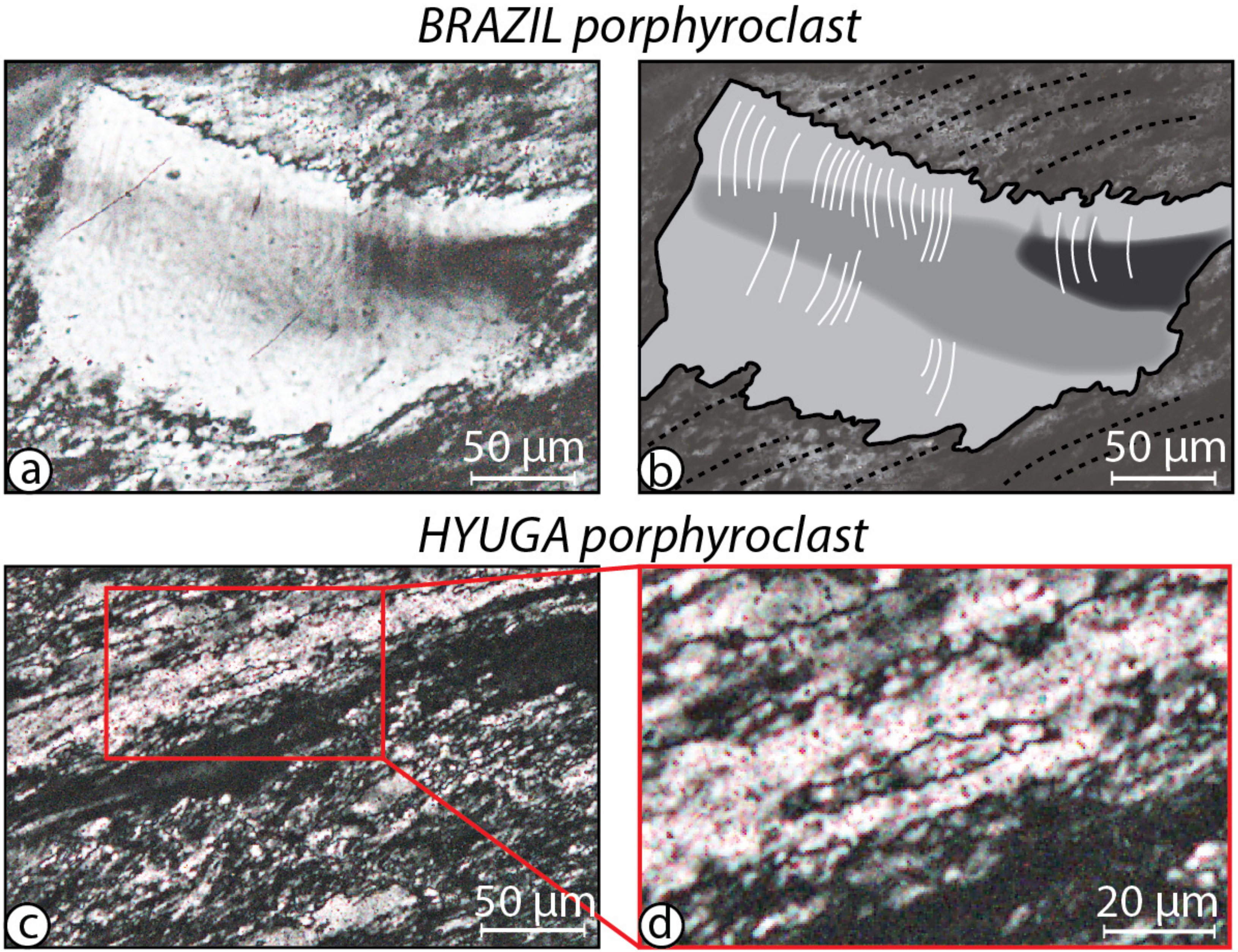
BRAZIL porphyroclast
a
50 μm
b
50 μm
HYUGA porphyroclast
c
50 μm
d
20 μm

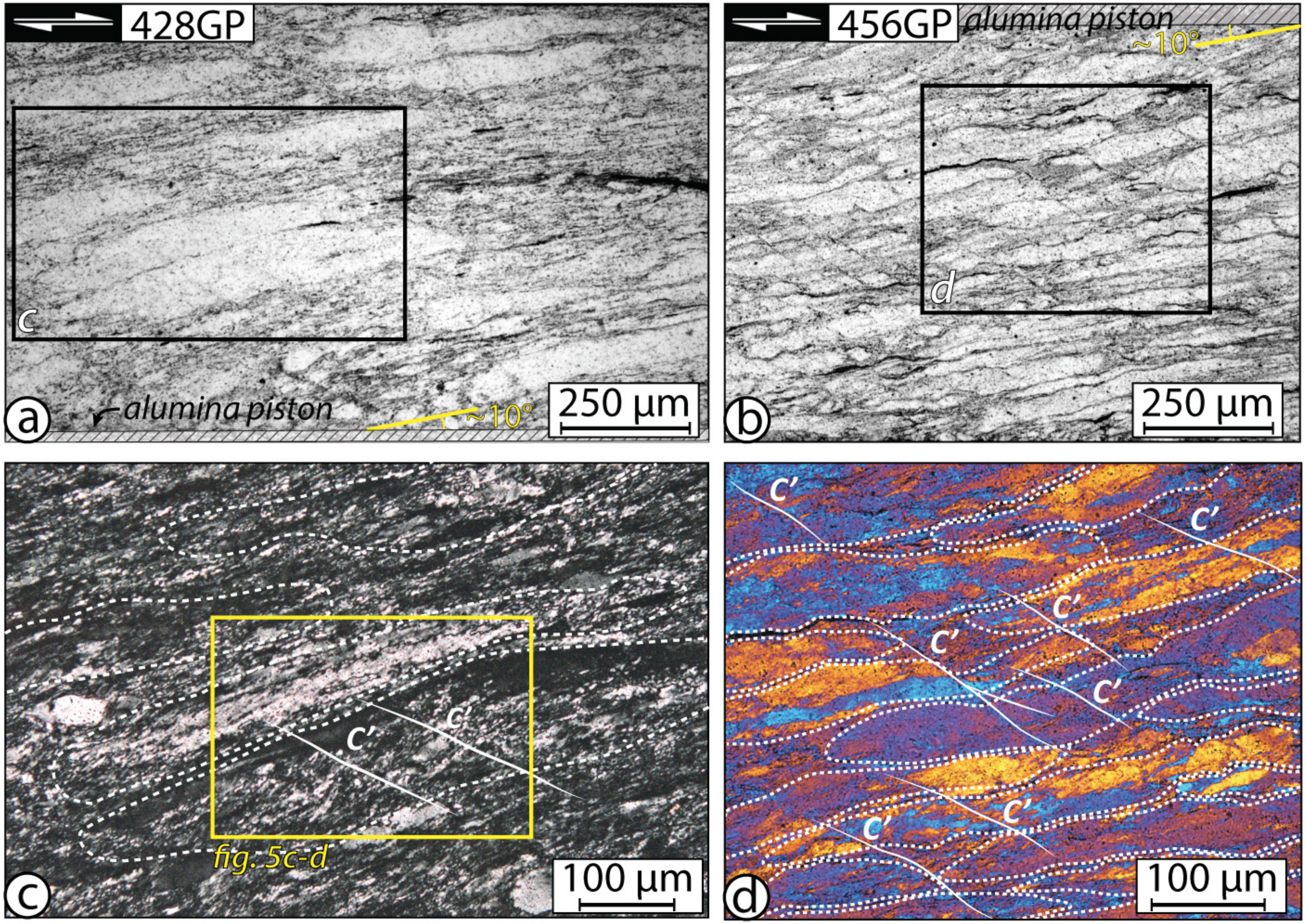

30 % HYUGA porphyroclasts

70 % HYUGA porphyroclasts

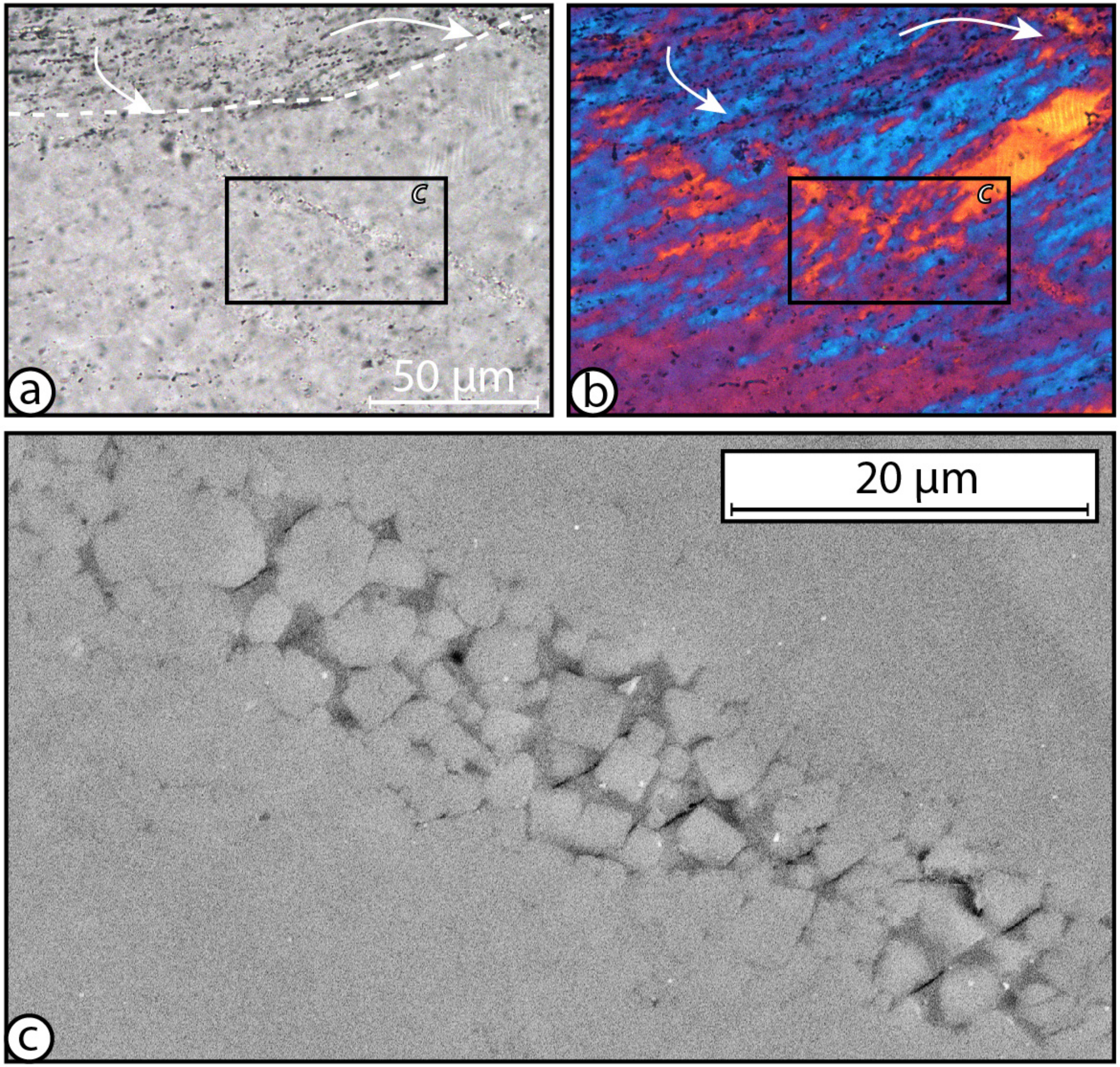
c
50 µm
a
c
b
20 µm
c

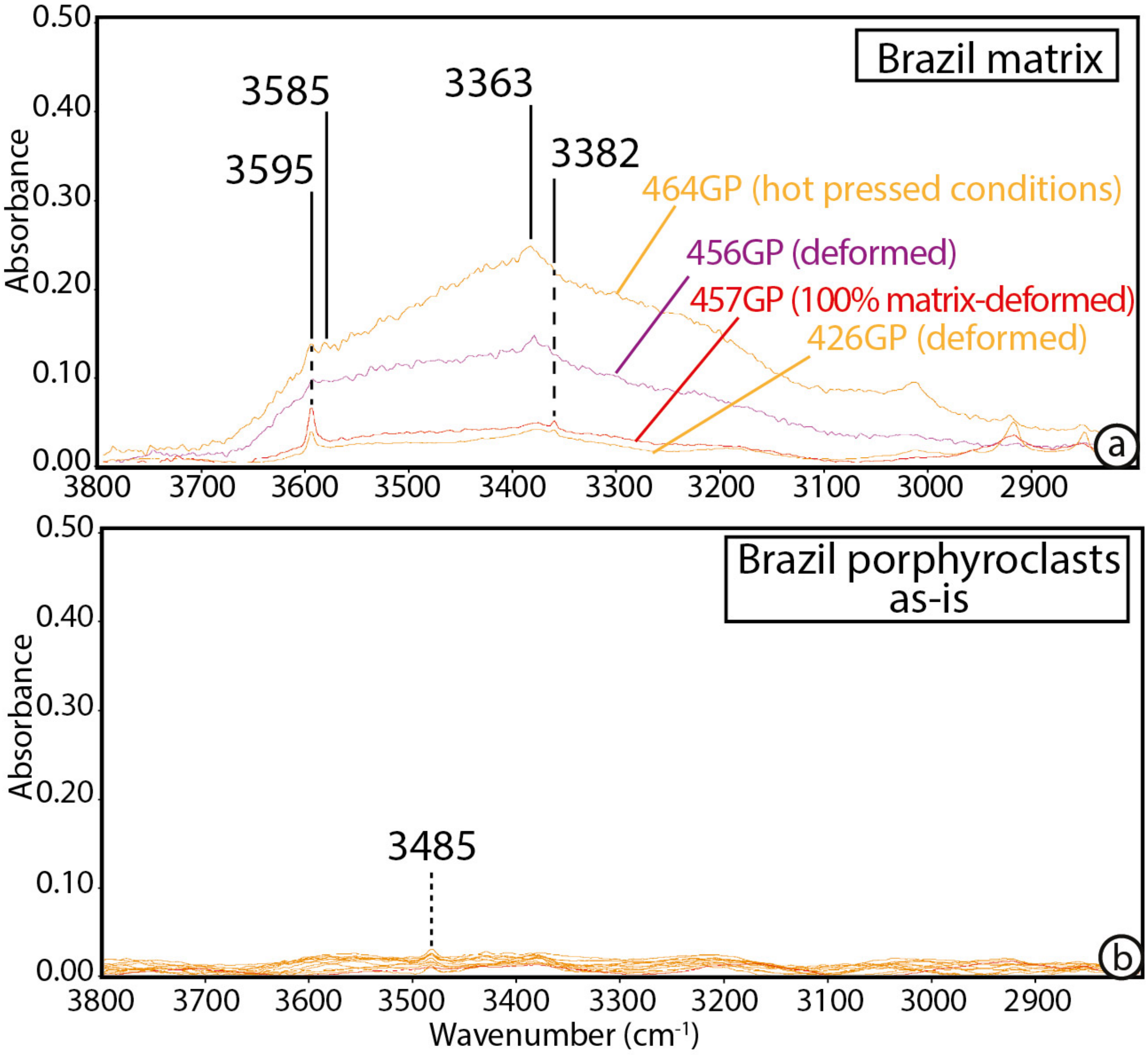
Brazil matrix
3585
3363
3595
3382
464GP (hot pressed conditions)
456GP (deformed)
457GP (100% matrix-deformed)
426GP (deformed)
a
Absorbance
0.50
0.40
0.30
0.20
0.10
0.00
3800
3700
3600
3500
3400
3300
3200
3100
3000
2900
Brazil porphyroclasts
as-is
3485
b
Wavenumber (cm-1)

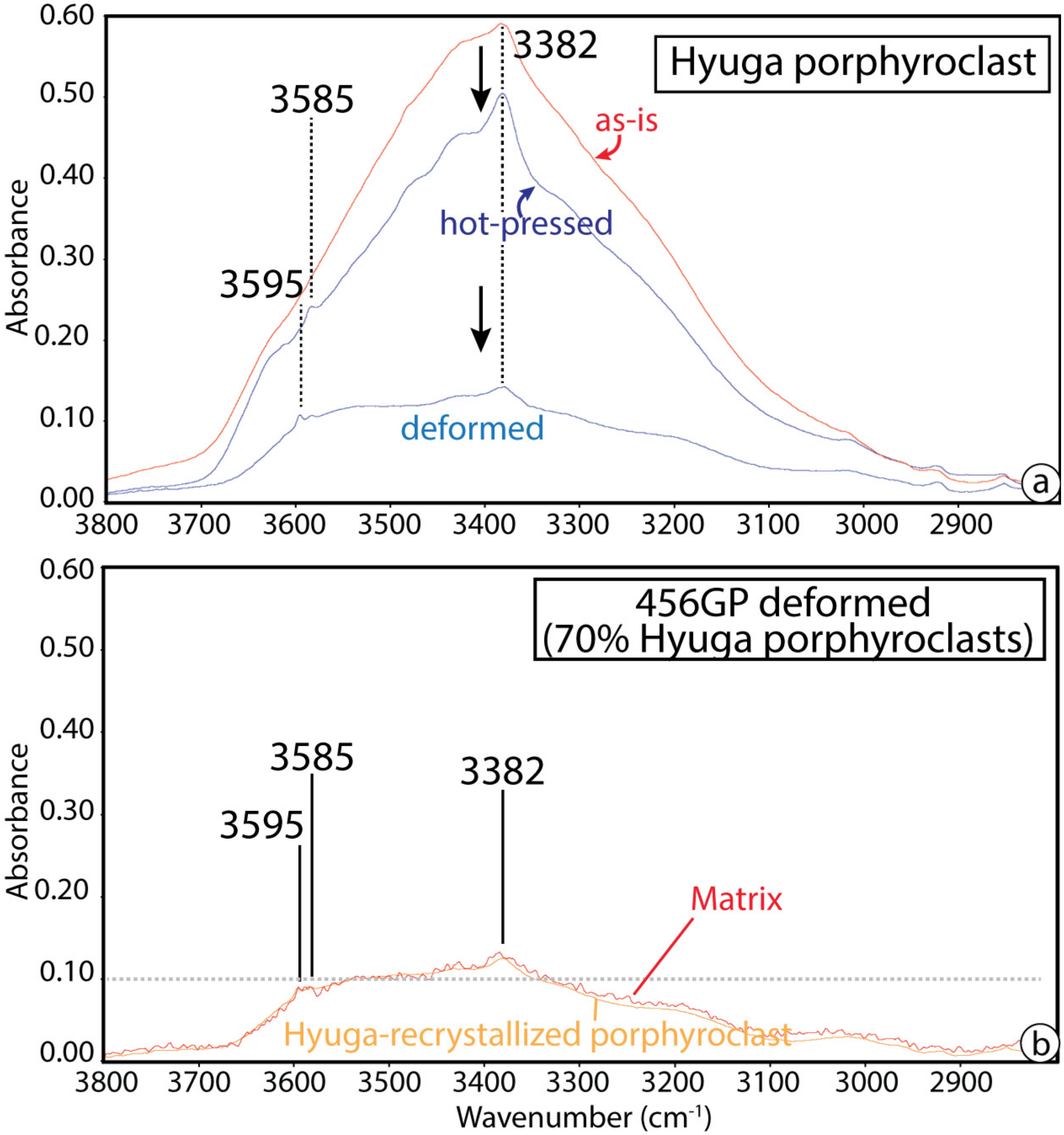
Hyuga porphyroclast
as-is
hot-pressed
deformed
3382
3585
3595
a
456GP deformed
(70% Hyuga porphyroclasts)
3585
3595
3382
Matrix
Hyuga-recrystallized porphyroclast
b
Absorbance
0.60
0.50
0.40
0.30
0.20
0.10
0.00
3800
3700
3600
3500
3400
3300
3200
3100
3000
2900
Wavenumber (cm^{-1})

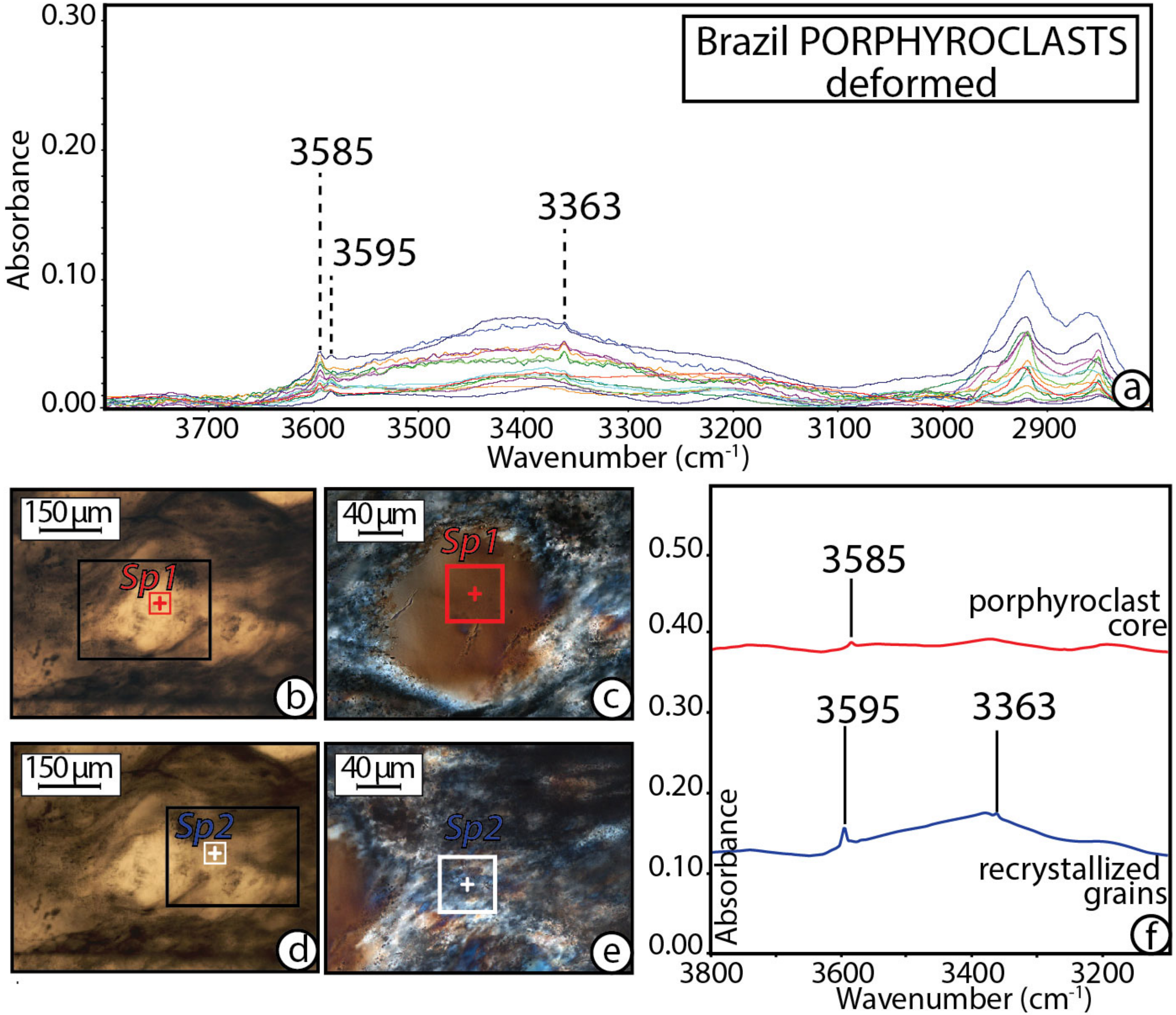
Brazil PORPHYROCLASTS deformed
3585
3595
3363
Absorbance
0.30
0.20
0.10
0.00
3700
3600
3500
3400
3300
3200
3100
3000
2900
Wavenumber (cm^{-1})
a
150 µm
Sp1
b
40 µm
Sp1
c
150 µm
Sp2
d
40 µm
Sp2
e
0.50
0.40
0.30
0.20
0.10
0.00
3585
porphyroclast core
3595
3363
recrystallized grains
Absorbance
3800
3600
3400
3200
Wavenumber (cm^{-1})
f

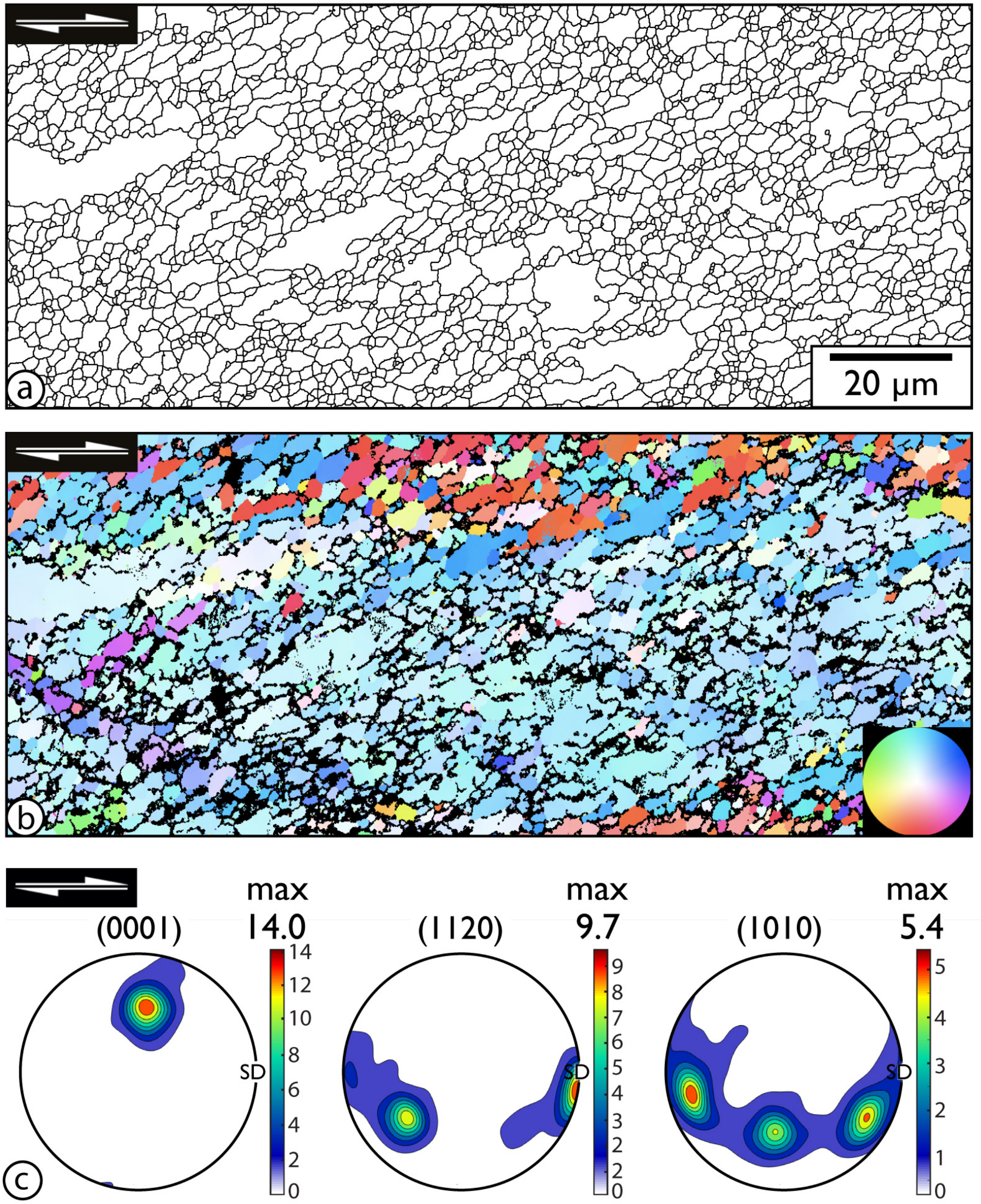
a
20 µm
b
c
max
(0001)
14.0
14
12
10
8
6
4
2
0
SD
max
(1120)
9.7
9
8
7
6
5
4
3
2
2
0
SD
max
(1010)
5.4
5
4
3
2
1
0
SD

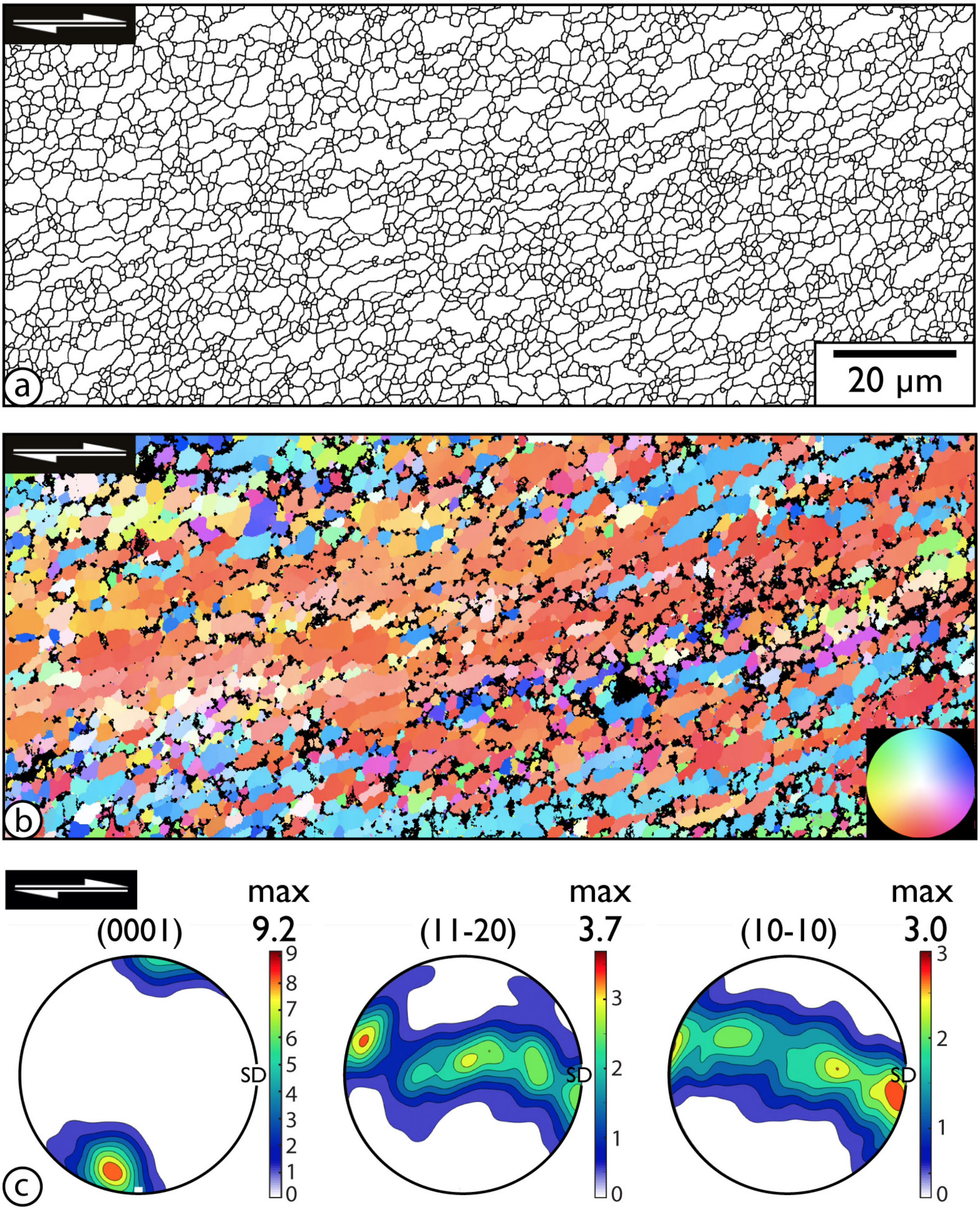
a
20 µm
b
c
max 9.2
(0001)
max 3.7
(11-20)
max 3.0
(10-10)
SD
SD
SD
0
1
2
3
4
5
6
7
8
9
0
1
2
3
0
1
2
3

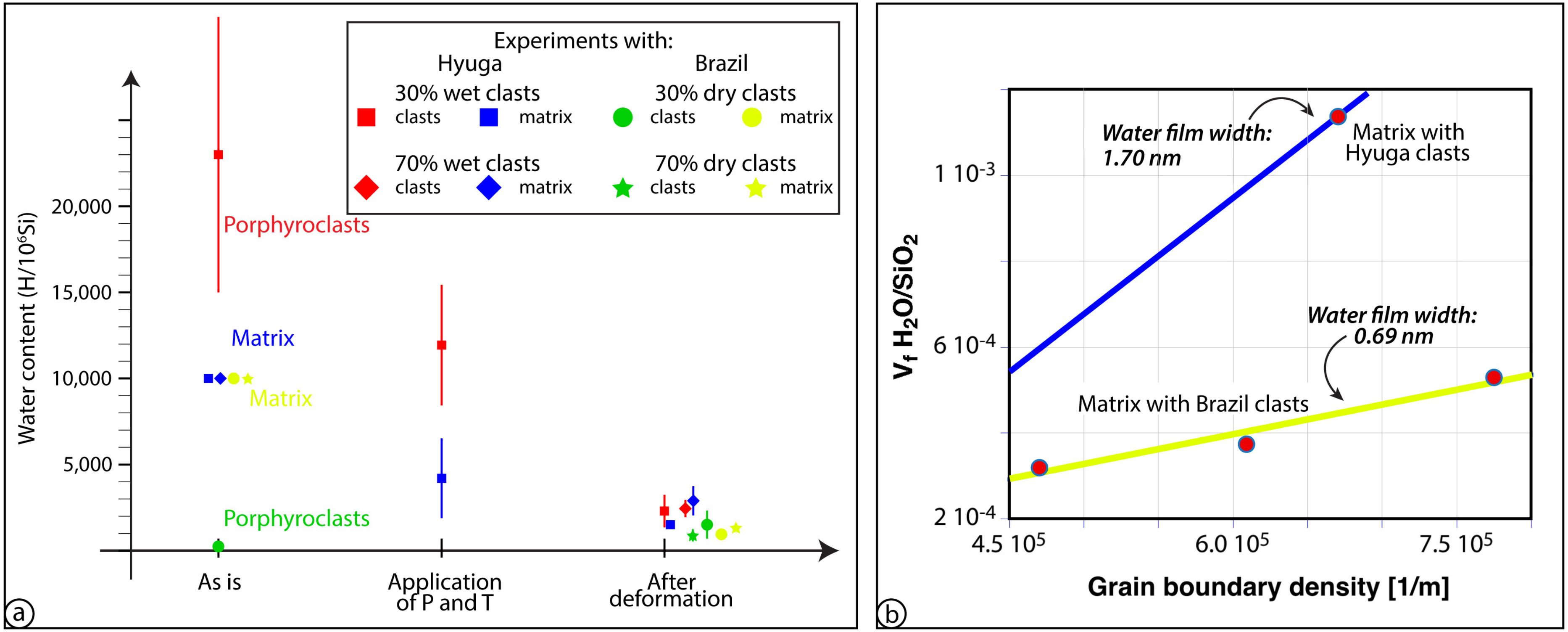
a
Water content (H/10^{6}Si)
20,000
15,000
10,000
5,000
As is
Application of P and T
After deformation
Porphyroclasts
Matrix
Matrix
Porphyroclasts
Experiments with:
Hyuga
Brazil
30% wet clasts
clasts
matrix
30% dry clasts
clasts
matrix
70% wet clasts
clasts
matrix
70% dry clasts
clasts
matrix
b
V_f H_2O/SiO_2
1 10^{-3}
6 10^{-4}
2 10^{-4}
4.5 10^5
6.0 10^5
7.5 10^5
Grain boundary density [1/m]
Water film width: 1.70 nm
Matrix with Hyuga clasts
Water film width: 0.69 nm
Matrix with Brazil clasts

Table 1 - Water content

Sample number	Composition of sample	Condition of sample	Measured material	Thickness (cm)	Abs (cm^2)	SD	wt. ppm H_2O	SD	wt. ppm $H/10^6$ Si	SD	Number of analyses
457GP	100% matrix	deformed	Matrix	0.0120	11.1	2.90	121	28	807	189	31
starting material	Hyuga porphyroclasts	as-is	Porphyroclast	0.0140	383.5	164.4	3446	1234	22973	8224	16
464GP	Hyuga porphyroclasts	attained P-T conditions	Core of porphyroclast	0.0133	191.2	56.2	1809	516	12058	3448	16
464GP	Matrix with Hyuga porphyroclasts	attained P-T conditions	Matrix	0.0127	63.9	34.7	633	344	4219	2296	10
428GP	Hyuga porphyroclasts	deformed	Porphyroclast	0.005	13.6	5.61	342	141	2278	941	8
428GP	Matrix with Hyuga porphyroclasts	deformed	Matrix	0.005	8.76	1.31	220	33	1469	220	9
428GP	Matrix with Hyuga porphyroclasts	deformed	Shear Bands	0.005	22.1	5.66	556	142	3710	949	12
456GP	Hyuga porphyroclasts	deformed	Recrystallized porphyroclast	0.0141	39,6	7.77	353	76	2355	509	15
456GP	Matrix with Hyuga porphyroclasts	deformed	Matrix	0.013	44.8	14.8	430	129	2868	863	9
starting material	Brazil porphyroclasts	as-is	Porphyroclast	0.0136	4.19	0.9	39	10	258	68	7
426GP	Brazil porphyroclasts	deformed	Core of porphyroclast	0.0123	9.36	6.18	96	68	638	455	13
426GP	Brazil porphyroclasts	deformed	Recrystallized porphyroclast	0.0118	21.5	14.9	229	131	1526	873	11
426GP	Matrix in Brazil sample	deformed	Matrix	0.0131	14.8	5.03	142	45	947	299	12
465GP	Brazil porphyroclasts	deformed	Recrystallized porphyroclast	0.0201	21.5	8.35	135	52	898	348	16
465GP	Matrix in Brazil sample	deformed	Matrix	0.0201	31.9	9.39	200	59	1332	391	24

Table 2-Mechanical Data

Sample number	**Composition of sample**	**% water added**	**$\dot{\gamma}$ [s^{-1}]**	**Peak τ [MPa]**	**γ at peak shear stress**	**τ at $\gamma = 3$ [MPa]**	**τ at end [MPa]**	**γ_{final}**
457GP	100% matrix	0.15	**2.21×10^{-5}**	**192**	**0.61**	**164**	**201**	**4.59**
462GP	“	“	**2.19×10^{-5}**	**307**	**0.78**	**247**	**256**	**3.54**
426GP	30% Brazil p.	0.10	**2.12×10^{-5}**	**421**	**0.81**	**286**	**271**	**3.30**
428GP	30% Hyuga p.	0.10	**2.08×10^{-5}**	**245**	**0.80**	**247**	**256**	**3.14**
465GP	70% Brazil p.	0.045	**2.17×10^{-5}**	**645**	**1.55**	**553**	**445**	**4.31**
456GP	70% Hyuga p.	0.045	**2.07×10^{-5}**	**398**	**0.69**	**277**	**292**	**3.87**
464GP	30% Hyuga p.	0.10	**0.5**	**-**	**-**		**-**	**-**
459GP	100% matrix	0.15	**18**	**-**	**-**		**-**	**-**

Table 3 - Absorption bands

			Absorption [cm^{-1}]						
Experiment	**Material**	**Conditions**	**3363**	**3385**	**3430**	**3485**	**3585**	**3595**	**3625**
-	Hyuga porphyroclasts	as-is		x	x	x			x
464GP	Hyuga porphyroclasts	attained P-T cond.		x	x	x	x		x
456GP	Hyuga porphyroclasts	deformed		x			x	x	
-	Brazil porphyroclasts	as-is				x			
426GP	Brazil porphyroclasts	deformed	x				x	x	
464GP	Matrix in Hyuga assembly	attained P-T cond.		x				x	
456GP	Matrix in Hyuga assembly	deformed		x				x	
426GP	Matrix in Brazil assembly	deformed	x					x	

Table 4- Grain boundary density

Experiment	**Composition of sample**	**Grain boundary density (1/m)**
457GP	100% matrix	**$4.7\ 10^5$**
456GP	70% Hyuga porphyroclasts	**$6.7\ 10^5$**
426GP	30% Brazil porphyroclasts	**$6.09\ 10^5$**
465GP	70% Brazil porphyroclasts	**$7.75\ 10^5$**

Aines, R.D., Rossman, G.R. (1984) Water in minerals? A peak in the infrared. J. Geophys. Res. Solid Earth 89, 4059–4071. doi:10.1029/JB089iB06p04059

Bakker, R.J. & Jansen, J.B.H. (1994) Contr. Mineral. and Petrol. 116: 7. doi.org/10.1007/BF00310686.

Blacic, J. D., and J. M. Christie (1984), Plasticity and hydrolytic weakening of quartz single crystals, J. Geophys. Res. Solid Earth, 89(B6), 4223–4239.

Chakraborty, D. & Lehmann, G. (1976). Distribution of OH in synthetic and natural quartz crystals. Journal of Solid State Chemistry 17, 305–311.

Christie, J. M., D. T. Griggs, and N. L. Carter (1964), Experimental evidence of basal slip in quartz, J. Geol., 734–756.

Cordier, P. and Doukhan, J.C. (1989) Water solubility in quartz and its influence on ductility. Eur. J. Mineral. 1, 221-237.

Cordier, P. and Doukhan, J.C. (1991) Water speciation in quartz: a near infrared study. American Mineralogist 76, 361-369.

de Ronde, A.A., Stünitz, H., Tullis, J. and Heilbronner, R. (2005) Reaction-induced weakening of plagioclase–olivine composites. Tectonophysics 409, 85-106.

Den Brok, B. (1998) Effect of microcracking on pressure-solution strain rate: The Gratz grain-boundary model. Geology 26, 915-918.

den Brok, B., J. Meinecke, and K. Roller (1994), Fourier transform IR-determination of intragranular water content in quartzites experimentally deformed with and without added water in the ductile deformation field, J. Geophys. Res., 99, 19,821–19,828.

Doukhan and Trépied, 1985. J.C. Doukhan, L. TrépiedPlastic deformation of quartz single crystals. Bull. Minér., 108 (1985), pp. 97-123.

Fitz Gerald, J.D., Boland, J.N., McLaren, A., Ord, A. and Hobbs, B.E. (1991) Microstructures in water-weakened single crystals of quartz. J. Geophys. Res. 96, 2139-2155.

Frondel, C. (1982), Structural hydroxyl in chalcedony (type B quartz), Am. Mineral., 67, 1248–1257.

Gerretsen, J., Paterson, M.S. and McLaren, A.C. (1989) The uptake and solubility of water in quartz at elevated pressure and temperature. Phys. Chem. Minerals 16, 334-342.

Gleason, G.C. and DeSisto, S. (2008) A natural example of crystal-plastic deformation enhancing the incorporation of water into quartz. Tectonophysics 446, 16-30.

Graetsch, H., Floerke, O.W., and G. Miehe (1985), The nature of water in chalcedony and opal-C from Brazilian agate geodes, Phys. Chem. Miner., 12(5), 300–306.

Graetsch, H., Floerke, O.W., and G. Miehe (1987), Structural defects in microcrystalline silica, Phys. Chem. Miner., 14(3), 249–257.

Griggs, D.T. (1967) Hydrolytic weakening of quartz and other silicates. Geophys. J. Roy. Astron. Soc. 14, 19-31.

Griggs, D.T. (1974) A model of hydrolytic weakening of quartz. J. Geophys. Res. 79, 1653-1661.

Griggs, D.T. and Blacic, J.D. (1965) Quartz: Anomalous weakness of synthetic crystals. Science 147, 292-295.

Hall, D.L. and Sterner, S.M. (1993) Preferential water loss from synthetic fluid inclusions. Contrib. Mineral. Petrol. 114, 489-500.

Hanmer, S. (1984b) The potential use of planar and elliptical structures as indicators of strain regime and kinematics of tectonic flow. Geol Surv Can Pap 84:133–142

Heilbronner, R., Tullis, J. (2006) Evolution of c axis pole figures and grain size during dynamic recrystallization: results from experimentally sheared quartzite. Journal of Geophysical Research-Solid Earth 111 (B10), B10202.

Heilbronner, R., and S. Barrett (2014), Image Analysis in Earth Sciences, pp. 520, Springer, Berlin.

Heilbronner, R. and Kilian, R. (2017) The grain size(s) of Black Hills Quartzite deformed in the dislocation creep regime, Solid Earth, 8, 1071–1093, **https://doi.org/10.5194/se-8-1071-2017**, Hielscher, R., and H. Schaeben (2008), A novel pole figure inversion method: Specification of the MTEX algorithm, J. Appl. Crystallogr., 41, 1024–1037, doi:10.1107/S0021889808030112. [Available at https://mtex-toolbox.github.io/.]

Hiraga, T., Anderson, I.M. and Kohlstedt, D.L. (2004) Grain boundaries as reservoirs of incompatible elements in the Earth's mantle. Nature 427, 699-703.

Hirth, G. and Tullis, J. (1992) Dislocation creep regimes in quartz aggregates. J. Struct. Geol. 14, 145-159.

Hirth, G., Teyssier, C., Dunlap, J.W., 2001. An evaluation of quartzite flow laws based on comparisons between experimentally and naturally deformed rocks. Int. J. Earth Sci. 90, 77–87. http://dx.doi.org/10.1007/s005310000152.

Ito, Y. and Nakashima, S. (2002) Water distribution in low-grade siliceous metamorphic rocks by micro-FTIR and its relation to grain size: a case from the Kanto Mountain region, Japan. Chem. Geol. 189, 1-18.

Jaoul, O., Tullis, J. and Kronenberg, A.K. (1984) The effect of varying water contents on the creep behavior of Heavitree quartzite. J. Geophys. Res. 89, 4298-4312.Kats, A. (1962). Hydrogen in alpha quartz. Philips Res. Rep. 17, 1–31; 133–195; 201–279.

Kekulawala, K.R.S.S., Paterson, M.S. and Boland, J.N. (1978) Hydrolytic weakening in quartz. Tectonophysics 46, T1--T6.

Kekulawala, K.R.S.S., Paterson, M.S. and Boland, J.N. (1981) An experimental study of the role of water in quartz deformation, in: Carter, N.L., et al. (Eds.), Mechanical behavior of crustal rocks, Geophys. Monogr. Ser., vol. 24. AGU, Washington, D. C., pp. 49-60.

Kidder, S., G. Hirth, J. P. Avouac, and W. Behr (2016), The influence of stress history on the grain size and microstructure of experimentally deformed quartzite, J. Struct. Geol., 83, 194–206.

Kilian, R., Heilbronner, R., Holyoke III, C.W., Kronenberg, A.K. and Stünitz, H. (2016) Dislocation creep of dry quartz. J. Geophys. Res. 121, 3278-3299.

Kilian, R., Heilbronner, R. (2017) Analysis of crystallographic preferred orientations of experimentally deformed Black Hills Quartzite Solid Earth, 8, 1095–1117, 2017.https://doi.org/10.5194/se-8-1095-2017

Kohlstedt, D. L., Evans, B. & Mackwell, S. J. Strength of the lithosphere: Constraints imposed by laboratory experiments. J. Geophys. Res. 100, 17587–17602 (1995).

Kronenberg, A.K. and Tullis, J. (1984) Flow strengths of quartz aggregates: Grain size and pressure effects due to hydrolytic weakening. J. Geophys. Res. 89, 4281-4297.

Kronenberg, A., S. Kirby, R. Aines, and G. Rossman (1986), Solubility and diffusional uptake of hydrogen in quartz at high water pressures: Implications for hydrolytic weakening, J. Geophys. Res., 91(B12), 2723–2744, doi:10.1029/JB091iB12p12723.

Kronenberg, A.K., Segall, P., Wolf, G.H., 1990. Hydrolytic weakening and penetrative deformation within a natural shear zone. Geophys. Monogr. 56, 21–36.

Law, R. D., Knipe, R. J. & Dayan, H. 1984. Strain path partitioning within thrust sheets: Microstructural and petrofabric evidence from the Moine Thrust zone at Loch Eriboll, northwest Scotland. J. Struct. Geol. 6, 477-497.

Law, R.D., 1990. Crystallographic fabrics: a selective review of their applications to research in structural geology. Geol. Soc. Lond. Spec. Publ. 54, 335–352. doi:10.1144/GSL.SP.1990.054.01.30

Lloyd, G.E., Freeman, B., 1994. Dynamic recrystallization of quartz under greenschist conditions. J. Struct. Geol. 16, 867–881. doi:10.1016/0191-8141(94)90151-1

Mainprice, D. and Jaoul, O. (2009) A transmission electron microscopy study of experimentally deformed quartzite with different degrees of doping. Phys. Earth Planet. In. 172, 55-66.

Marti, S., H. Stünitz, R. Heilbronner, O. Plümper, and M. Drury (2017), Experimental investigation of the brittle-viscous transition in mafic rocks - Interplay between fracturing, reaction, and viscous deformation, J Struct Geol 105:62-70, doi.org/10.1016/j.jsg.2017.10.011.

Menegon, L., P. Nasipuri, H. Stünitz, H. Behrens, and E. Ravna (2011), Dry and strong quartz during deformation of the lower crust in thepresence of melt, J. Geophys. Res., 116, B10410, doi:10.1029/2011JB008371.

McLaren, A.C., Cook, R.F., Hyde, S.T. and Tobin, R.C. (1983) The mechanisms of the formation and growth of water bubbles and associated dislocation loops in synthetic quartz. Phys. Chem. Minerals 9, 79-94.

McLaren, A.C., Fitz Gerald, J.D. and Gerretsen, J. (1989) Dislocation nucleation and multiplication in synthetic quartz: relevance to water weakening. Phys. Chem. Minerals 16, 465-482.

Nakashima, S. (1995) Diffusivity of ions in pore water as a quantitative basis for rock deformation rate estimates. Tectonophysics 245, 185-203.

Nakashima, S., Matayoshi, H., Yuko, T., Michibayashi, K., Masuda, T., Kuroki, N., Yamagashi, H., Ito, Y. and Nakamura, A. (1995) Infrared microspectroscopy analysis of water distribution in deformed and metamorphosed rocks. Tectonophysics 245, 263-276.

Niimi, N., Aikawa, A. and Shinoda, K. (1999) The infrared absorption band at 3596 cm-1 of the recrystallized quartz from Mt. Takamiyama, southwest Japan. Mineral. Mag. 63, 693-701.Olgaard, D.L., Fitz Gerald, J.D., 1993. Evolution of pore microstructures during healing of grain boundaries in synthetic calcite rocks. Contributions to Mineralogy and Petrology 115, 138e154.Palazzin, G., Raimbourg, H., Famin, V., Jolivet, L., Kusaba, Y. and Yamaguchi, A. (2016) Deformation processes at the down-dip limit of the seismogenic zone: The example of Shimanto accretionary complex. Tectonophysics 687, 28-43.

Palazzin, G., Raimbourg, H., Famin, V., Jolivet, L., Kusaba, Y. and Yamaguchi, A. (2016) Deformation processes at the down-dip limit of the seismogenic zone: The example of Shimanto accretionary complex. Tectonophysics 687, 28-43.

Pankrath, R. (1991) Polarized IR spectra of synthetic smoky quartz. Phys. Chem. Minerals 17, 681-689.

Passchier CW, Simpson C (1986) Porphyroclast systems as kinematic indicators. J Struct Geol 8:831–844.

Paterson, M. S. (1986), The thermodynamics of water in quartz, Phys. Chem. Miner., 13(4), 245–255.

Paterson, M. S. (1989), The interaction of water with quartz and its influence in dislocation flow: an overview, Rheol. Solids Earth, 107–142.

Paterson, M. S., B. E. Hobbs, and A. C. McLaren (1972), The plasticity of single crystals of synthetic quartz, Transactions of the American Geophysical Union (USA), American Geophysical Union 53rd Annual Meeting, vol. 53, pp. 514–15, AGU, Washington, D. C., 17–21 Apr.

Pec, M., H. Stünitz, R. Heilbronner, and M. Drury (2016), Semi-brittle flow of granitoid fault rocks in experiments at mid-crustal conditions, J. Geophys. Res. Atmos., 121, 1677–1705, doi:10.1002/2015JB012513.

Post, A. and Tullis, J. (1998) The rate of water penetration in experimentally deformed quartzite: implications for hydrolytic weakening. Tectonophysics 295, 117-137.

Prior, D.J. (1999). Problems in determining the misorientation axes, for small angular misorientations, using electron backscatter diffraction in the SEM. J. Microsc.-Oxford 195, 217–225.

Raimbourg, H., Kogure, T. and Toyoshima, T. (2011) Crystal bending, subgrain boundary development, and recrystallization in orthopyroxene during granulite-facies deformation. Contrib. Min. Petr. 162(5), doi:10.1007/s00410-00011-00642-00413.

Raimbourg, H., Famin, V., Palazzin, G., Mayoux, M., Jolivet, L., Ramboz, C. and Yamaguchi, A. (2018) Fluid properties and dynamics along the seismogenic plate interface. Geosphere: Subduction top to bottom 2 14, 1-23.

Raimbourg, H., Vacelet, M., Ramboz, C., Famin, V., Augier, R., Palazzin, G., Yamaguchi, A. and Kimura, G. (2015) Fluid circulation in the depths of accretionary prisms: an example of the Shimanto Belt, Kyushu, Japan. Tectonophysics 655, 161-176.Raimbourg, H., R. Augier, V.

Famin, L. Gadenne, G. Palazzin, A. Yamaguchi, and G. Kimura (2014), Long-term evolution of an accretionary prism: The case study of the Shimanto Belt, Kyushu, Japan, Tectonics, 33, 936–959, doi:10.1002/2013TC003412.

Richter, B., H. Stünitz, and R. Heilbronner (2016), Stresses and pressures at the quartz-to-coesite phase transformation in shear deformation experiments, J. Geophys. Res. Solid Earth, 121, doi:10.1002/2016JB013084.

Rovetta, M.R., Holloway, J.R. and Blacic, J.D. (1986) Solubility of hydroxyl in natural quartz annealed in water at 900°C and 1.5GPa. Geophys. Res. Lett. 13, 145-148.

Rovetta, M.R., 1989. Experimental and spectroscopic constraints on the solubility of hydroxyl in quartz. Phys. Earth Planet. Inter. 55, 326–334. doi:10.1016/0031-9201(89)90080-0

Rutter, E. H. & Brodie, K. H. Experimental grain size-sensitive flow of hot-pressed Brazilian quartz aggregates. Journal of Structural Geology 26, 2011–2023 (2004).

Saffer, D. M. & Tobin, H. J. Hydrogeology and Mechanics of Subduction Zone Forearcs: Fluid Flow and Pore Pressure. *Annual Review of Earth and Planetary Sciences* 39, 157–186 (2011)

Stalder, R. and Konzett, J. (2012) OH defects in quartz in the system quartz–albite–water and granite–water between 5 and 25 kbar. Phys. Chem. Minerals 39, 817-827.

Schmatz, J., Urai, J.L., 2010. The interaction of fluid inclusions and migrating grain boundaries in a rock analogue: deformation and annealing of polycrystalline camphor-ethanol mixtures. J. Metamorph. Geol. 28, 1–18. doi:10.1111/j.1525-1314.2009.00849.x

Schmid, S.M., Casey, M., 1986. Complete fabric analysis of some commonly observed quartz C-axis patterns. In: Hobbs, B.E., Heard, H.C. (Eds.), Mineral and Rock Deformation: Laboratory Studies. American Geophysical Union Monograph, vol. 36, pp. 263–286.

Schmocker, M. *et al.* Granular flow and Riedel band formation in water-rich quartz aggregates experimentally deformed in torsion. *J. Geophys. Res.* 108, 2242 (2003).

Stipp, M. and Tullis, J. (2003) The recrystallized grain size piezometer for quartz. Geophys. Res. Lett. 30, doi:10.1029/2003GL018444.

Stolper, E., 1982. The speciation of water in silicate melts. Geochim. Cosmochim. Acta 46, 2609–2620. doi:10.1016/0016-7037(82)90381-7

Stünitz, H., Thust, A., Heilbronner, R., Behrens, H., Kilian, R., Tarantola, A. and Fitz Gerald, J. (2017) Water redistribution in experimentally deformed natural milky quartz single crystals—Implications for H2O-weakening processes. J. Geophys. Res. 122, 866-894.

Tarantola, A., Diamond, L.W. and Stünitz, H. (2010) Modification of fluid inclusions in quartz by deviatoric stress I: experimentally induced changes in inclusion shapes and microstructures. Contrib. Mineral. Petrol. 160, 825-843.

Tarantola, A., L. W. Diamond, H. Stünitz, A. Thust, and M. Pec (2012), Modification of fluid inclusions in quartz by deviatoric stress. III: influence of principal stresses on inclusion density and orientation, Contrib. to Mineral. Petrol., 164(3), 537–550.

Trepmann, C. A. & Stöckhert, B. Quartz microstructures developed during non-steady state plastic flow at rapidly decaying stress and strain rate. Journal of Structural Geology 25, 2035–2051 (2003).

Tullis, J. and Yund, R.A. (1989) Hydrolytic weakening of quartz aggregates: The effect of water and pressure and recovery. Geoph. Res. Lett. 16, 1343-1346.

Vityk, M.O. and Bodnar, R.J. (1995) Textural evolution of synthetic fluid inclusions in quartz during reequilibration, with applications to tectonic reconstruction. Contrib. Mineral. Petrol. 121, 309-323.

Yamagishi, H., Nakashima, S., Ito, Y., 1997. High temperature infrared spectra of hydrous microcrystalline quartz. Phys. Chem. Miner. 24, 66–74. doi:10.1007/s002690050018.

Wood, D. L. (1960), Infrared absorption of defects in quartz, J. Phys. Chem. Solids, 13(3), 326–336.

Figure 1

a) Schematic representation of the sample assembly used in this study, before and after deformation, showing the piston final positions and the state of the deformed porphyroclasts + matrix mixture. Blue color indicates high strain deformed sample.

b) Characterization of the concentration in water in different starting materials, using FTIR spectrum centered on the water absorption band. Note that in 2 the absorption scale is expanded to account for the very low water concentration. All images are plane polarized light microscope images.

1. Hyuga porphyroclasts (p): tiny fluid inclusions are extremely abundant and cause a dark appearance of the porphyroclasts. Their distribution is heterogeneous within each single grain, resulting in different IR absorbance. Grains show fractures caused by mechanical crushing.
2. Experimental assembly with 30% Hyuga porphyroclasts (p) (464GP) embedded in the Brazil quartz matrix (m), after hydrostatic hot pressing at 800°C and 1.5 GPa: fluid inclusions abundance inside porphyroclasts is decreased with respect to the initial stage (fig.1a), producing lower absorbance values.
3. Brazil quartz porphyroclasts (p): clasts are clear and contain no fluid inclusions. IR spectra show a very low absorbance.

Figure 2

Shear stress–shear strain curves for the samples deformed in this study; for final stress values see Table 2. The star and the red circle correspond to shear stress calculated for our experimental conditions (800°C, 1.5GPa and strain rate of 2.1 x $10^{-5}s^{-1}$) using the flow laws of Hirth et al. (2001) and Paterson and Luan (1990) respectively.

Figure 3

BSE images of the matrix composed of Brazil quartz after "hot-pressing" stage (confining pressure 1.5 GPa; T=800°C). Porosity is observed at triple junctions between polygonal grains (white arrows) and at open grain boundaries (yellow arrow) from unloading. White particles are dust particles.

Figure 4

Microstructures of matrix+Brazil porphyroclasts assemblies after deformation.

a. Matrix + 30 % porphyroclasts (426GP). Brazil porphyroclasts are quite variable in shape, from highly stretched (at the piston contact) to equant shape. Foliation develops at about 18° from the shear zone boundary (forcing block interface).
b. Matrix + 70% porphyroclasts (465GP). Porphyroclasts are composed of a core, with an equant shape, and stretched tails.
c. Close up on some Brazil porphyroclasts (426GP). Porphyroclasts have angular edges. Internally they show deformation lamellae (central lower

white porphyroclast) and undulatory extinction (grain in the upper right corner) (see also fig. 5a-b).

d. Close up on some Brazil porphyroclasts (465GP). Porphyroclast cores show no subgrains but commonly undulatory extinction and deformation lamellae. Porphyroclast outer rims and tails are composed of very small recrystallized grains with different orientation from the core.

Plane polarized light (a-b), cross-polarizers (c) and cross-polarizers with compensation plate (d), all light microscope images. Dextral shear sense for all images.

Figure 5

Deformation microstructures within the porphyroclasts.

a-b) Close-up view of the deformed Brazil quartz porphyroclast in fig. 4c. Note the sutured porphyroclast boundaries (black lines), the undulatory extinction, the deformation lamellae (white lines), and foliation in the surrounding matrix (dashed black lines).

c-d) Close-up view of the deformed Hyuga porphyroclasts in fig. 6c. These porphyroclasts are composed of elongated subdomains limited by sutured grain boundaries. These subdomains are made up of small recrystallized (sub)grains distinguishable by thier crystal orientations.

Cross-polarizers, all light microscope images, (a, c, d) and interpretative sketch (b).

Figure 6

Microstructures of matrix + Hyuga porphyroclasts assemblies after deformation.

a) Matrix + 30 % porphyroclasts (428GP). Porphyroclasts are easily distinguishable from matrix because of their clearer appearance. Foliation is defined by the alignment of porphyroclasts and develops at ~10° from the shear zone boundaries. All porphyroclasts are strongly elongated. Note the presence of larger clasts in the matrix.

b) Matrix + 70 % porphyroclasts (456GP). Hyuga porphyroclasts are strongly elongated with an aspect ratio up to 10:1.

c) and d), C' Shear bands (highlighted with white lines), synthetic to the dextral shear sense, cut across the porphyroclasts (highlighted with dashed white lines) and matrix, making an angle of 25-30° from the shear zone boundaries (forcing block interface). Some internal domains of porphyroclasts preserve an internal coherence (fig. 5c-d), in terms of crystallographic orientation, in spite of extensive recrystallization (yellow domains).

Plane polarized light (a-b), cross-polarizers (c) and cross-polarizers with compensation plate (d), all light microscope images. Dextral shear sense for all images.

Figure 7

Shear bands developed in sample 456GP (70% Hyuga porphyroclasts).

a) Shear bands (orientation indicated by the white arrows) contain abundant porosity and cut across the matrix and a porphyroclast. The matrix and the

porphyroclast are in the upper and lower portion of the image separated by the dashed white line.
b) Shear bands show different crystal orientation, visible from their different extinction color (yellow) with respect to the surrounding porphyroclast.
c) Shear bands are made up of equant and faceted grains, a few microns in size, separated from one another by void space. The large porosity of the shear band is in contrast with the surrounding porphyroclast, where there is no porosity. Plane polarized light (a), crossed-polarizers with compensation plate (b), all light microscope images, SEM image (c).

Figure 8
FTIR spectra of Brazil quartz in (a) matrix material (at the end of the experiments), and (b) original starting material. Prior to all experiments, a 0.15 wt% H_2O was added to the matrix. At the end of all the experiments, the matrix is enriched in water with respect to the dry Brazil quartz powder; in other words, the matrix has retained a fraction of the initially added water. All experimental material has been deformed to large shear strain, except for 464GP, which has been subjected to the same P,T-conditions as those of the deformation experiments for ~30 min. The highest amounts of water are found in the experiments with Hyuga porphyroclasts. In addition, water concentration is highest in the experiment without deformation. Note the discrete absorption band at 3595 cm^{-1} in all experimental samples. The band at 3382 cm^{-1} is associated with the matrix in experiments with Hyuga clasts, while the band at 3363 cm^{-1} is associated with the matrix in experiments with Brazil porphyroclasts. “As-is” Brazil quartz shows only a discrete absorption band at 3485 cm^{-1}.

Figure 9
Effect of the application of P-T and deformation on the water content of Hyuga porphyroclasts, containing initially a large number of fluid inclusions.
a) Evolution of water concentration and absorption bands in Hyuga porphyroclasts ‘as-is’ (red), ‘hot-pressed’ (dark blue) and ‘deformed’ (blue) (all spectra are represented with the same scale). Note the important sharpening in discrete absorption bands from the ‘as-is’ to the ‘hot pressed’ material. Most of initial discrete bands disappear with deformation while a new band is detected at 3595 cm^{-1}.
b) Comparison of water amount between a recrystallized Hyuga porphyroclast and the surrounding matrix. The two FTIR spectra show a similar absorbance, the same shape and the same discrete absorption bands.

Figure 10
Water concentration and speciation in deformed Brazil porphyroclasts.
(a) FTIR spectrum of Brazil porphyroclasts, showing three discrete bands at 3595, 3585, 3363 cm^{-1}. Each color indicates a single measurement.
(b, c, d,e,f) Relationship between FTIR spectra and microstructures. The red spectrum in (f) corresponds to a porphyroclast core (red square in (b) and (c),

labelled “Sp1”), while the blue spectrum corresponds to its recrystallized tail (white square in (d) and (e), labelled “Sp2”) made of grains of ~4µm in size. Recrystallized tails of porphyroclasts contain a much higher water concentration than their core. In addition, they show a peak around 3595cm^{-1}, contrasting with the peak around 3585cm^{-1} present in the core. Plane polarized light (b, d) and crossed polarizers (c, e), light microscope images.

Figure 11
Microstructure and texture of pure matrix. Central part of sample 457GP. The shear sense is dextral, top to the right; SD is the shear direction.
a) Grain boundary map obtained by segmentation of EBSD map based on c-axis orientation after conversion to CIP images: in order to best reproduce the visual identification of grains, segmentation is performed using c- axis misorientation angle of 3°,which is approximately equivalent to a full misorientation angle of 5°.
b) Orientation image with color look-up table (LUT) for c-axis orientations in the Z-direction.
c) Pole figures for c- a- and m- directions; maximum density of each axis are indicated above color bar; contours are at intervals of uniform density (m.u.d); SD: shear direction.

Figure 12
Microstructure and texture of experiment with 70% of Hyuga porphyroclasts. Central part of sample 456GP. Dextral shear is applied.
Description of a) b) and c) are the same as figure 11.

Figure 13
Microstructure and texture of experiment with 70% of Brazil porphyroclasts. Central part of sample 465GP. Dextral shear is applied.
Description of a) b) and c) are the same as figure 11.

Figure 14
a) Water contents of samples before and after deformation. Water amount for Brazil porphyroclasts refers to recrystallized zones. All values are measured by FT-IR (see Table 1) except for ‘as-is’ matrix values which are calculated from the initial amounts of dry Brazil matrix powder and added water. b) H_2O volume fraction in quartz aggregates against grain boundary fraction of the analyzed volume. Volume fraction was calculated from FT-IR measurements of weight proportions of water (Table 1), assuming a density of 1 and 2.6 g/cm^3, for water and quartz, respectively. The slope of the regression curves represent some average thickness of the water film along the grain boundary estimated to ~0.7 nm for the pure matrix and the matrix with Brazil clasts and to ~1.70 nm for the matrix with Hyuga clasts.

Table 1
Molecular water content of Hyuga and Brazil porphyroclasts, Brazil matrix at different conditions: “as-is”, “hot-pressed” and “deformed”. (Th=thickness; Mean Abs= integrated absorbance area; wt. ppm= part par million weight; H/10^6 Si; SD = Standard Deviation). Stolper (1982) and Kats (1962) calibration.

Table 2
Deformation conditions (deformation time, gamma, peak stress and final stress values) and sample parameters (assembly, added H2O) of all deformation experiments. Confining pressure (Pc) = 1.5 GPa; Temperature (T) =800°C; strain rate = $2.1*10^{-5}$ s^{-1}.

Table 3
Absorption bands and associated materials with respect to experimental deformation conditions.

Table 4
Grain boundary density (surface/volume) calculated from grain boundary maps in Figs. 11 to 13.